Carbohydrate Polymer Technologies and Applications 16 (2026) 101237

Contents lists available at ScienceDirect

Carbohydrate Polymer Technologies and Applications

journal homepage: www.sciencedirect.com/journal/carbohydrate-polymer-technologies-and-applications

# Tailoring starch particle morphology through enzymatic, precipitation and spray-drying techniques as sustainable microplastic alternatives in cosmetics

Giulia Sinesi [a], Gaetano Distefano [b], Lucia Morelli [a,c], Lucia Salvioni [a,c], Patrizia Valsesia [b], Davide Prosperi [a,c,*], Marco Giustra [a,c,*], Miriam Colombo [a,c]

[a] NanoBioLab, Department of Biotechnology and Bioscience, University of Milano Bicocca, Milan, Italy
[b] Research & Innovation Department, Intercos SpA, Agrate Brianza, 20864, Italy
[c] Nanobiotechnologies for Health Center, NANOMIB, University of Milano-Bicocca, Milan, Italy

ARTICLE INFO

*Keywords:*
Cosmetic powders
Angle of repose
Powder flowability
Anti-solvent precipitation
α-Amylase surface erosion
Spray-drying

ABSTRACT

Microplastics have long been employed in cosmetic formulations to enhance sensory properties. However, growing environmental concerns necessitate sustainable alternatives as stated in the Regulation (EU) 2023/2055. Starch, an abundant and biodegradable polysaccharide, represents a promising candidate, yet its native form exhibits poor tactile aesthetics, limiting its application in high-end cosmetic products. Starches are powders widely used in cosmetics as humectants, absorbents, skin protectants, and viscosity adjusters. However, their irregular shape and "gritty" sensory perception have limited their use in formulations, leading to the widespread use of microplastics such as Nylon, PP, and PMMA for decades. This study investigates strategies to modify starch morphology and improve its sensory attributes for cosmetic use. Corn, tapioca, and mung bean starches were processed through enzymatic hydrolysis, freeze-drying, microprecipitation, and spray-drying to generate four distinct particle architectures: deflated spheres, sheets, smooth microparticles, and donut-like structures. Characterization was performed using scanning electron microscopy and angle-of-repose measurements. Results indicate that these modifications enhanced tactile smoothness and aesthetic performance, positioning these biopolymer matrices as promising sustainable alternatives to replace synthetic microbeads in cosmetic formulations. These reproducible and scalable protocols demonstrate that morphologically modified starch-based powders can serve as effective, eco-friendly substitutes for microplastics, aligning with sustainability goals without compromising quality.

## 1. Introduction

Microplastics (MPs) are small plastic fragments between 5.0 and 0.1 μm and denote a growing environmental issue, as they significantly impact the ecosystem. More specifically, as stated in Regulation (EU) 2023/2055, MPs are legally defined as "tiny fragments of synthetic or chemically modified natural polymers, which are insoluble in water, degrade very slowly and can easily be ingested by living organisms".(The European Commission, 2023) Indeed, due to their dimensions, they are difficult to filter out in the wastewater treatment plants, quickly reaching rivers, seas, and oceans.(Emenike et al., 2022; Samanta et al., 2022; Xu et al., 2021) Here, MPs can be consumed by marine animals or other biota.(Cubas et al., 2022)

Properties, texture, size, microbeads, fragments, nurdles, and foam classify microplastics.(Siddiqui et al., 2020) Cosmetic products, including creams, lotions, and personal care products added as ingredients represent a globally widespread MP source. MPs can occur either in a primary (directly incorporated in a cosmetic formulation) or in a secondary form (being a part of the packaging).(Ju et al., 2021) Regarding the first category, microplastics can be further divided into larger MPs — the particles used in exfoliants, abrasives, and rinse-off products — and smaller MPs, which are used to improve texture and are found in leave-on products. They are commonly employed to modulate product properties, typically within a size range of approximately 0.5-25 μm. Based on their form (*e.g.*, micro-pearls and powders), MPs can be exploited as texture/sensory modifiers, abrasives, and

* Corresponding authors.
*E-mail addresses:* davide.prosperi@unimib.it (D. Prosperi), marco.giustra@unimib.it (M. Giustra).

https://doi.org/10.1016/j.carpta.2026.101237

Available online 7 September 2026

exfoliants.(Tian et al., 2022) However, the pollution caused by these particles is due to improper disposal. This initial process facilitates their entry into the food chain, encompassing animals and spices. Several studies have highlighted the presence of these particles in the human body, including brain, liver, and genital organs, with a high likelihood of causing inflammation or disease.(Enyoh et al., 2020, 2023) Microplastics can accumulate in various human organs and the main types commonly used in cosmetic formulations have been identified. Among these, Nylon (polyamides), polyacrylates, and cross-linked polymers of synthetic materials are prevalent due to their advantageous physicochemical properties previously discussed.(Giustra et al., 2024) One of the claims is the need to find sustainable alternatives at both environmental and industrial levels. Starch is one of those that largely satisfy the criteria for operating in an eco-friendly environment. It is widely accepted because it is readily biodegradable and does not qualify as a synthetic polymer, as it complies with the OECD 301 standard.("OECD," 1992) It is already used in cosmetics as an absorbent, anticaking, humectant, film-forming, thickener, and viscosity control, finding large applicability in products such as face powders, dry shampoos, creams, powder eyeshadow, deodorants, lip balms, and face masks.(Gupta et al., 2022; Lochhead, 2007; Suhagia et al., 2025)

Starch is a polysaccharide composed of linear chains, the amylose α-D-(1,4) bonds, and branched ones α-D-(1,4) bonds and α-D-(1,6) bonds, the amylopectin. The properties of starches are influenced by the size, shape, and arrangement of the starch granules, as well as by the presence of amylose and amylopectin (Figure 1A and B). Indeed, amylose tends to retrograde, forming strong films and tough gels, while amylopectin forms weak films and soft gels. (Pérez & Bertoft, 2010; Puri et al., 2025) The morphology of native starch particles is closely related to their plant origin, as shown in Figure 1C-E. These irregular and/or lamellar particles are the cause of an interaction with the skin that is perceived, in many cases, as unpleasant from a sensory standpoint. Instead, a spherical shape is preferred thanks to the "ball bearing" effect, which allows for a sophisticated sensoriality. Furthermore, these particles have optical properties suitable for achieving a smoothing effect ("soft-focus"). Shape, size, and monodisperse distribution are interrelated properties that modulate the sensoriality of touch. (Petsitis, 2018; Shebalin, 2021)

Various techniques are useful for modifying the morphology of particles from different origins through treatments such as solubilization, precipitation, drying, sieving, and more. In this study, three types of starches from different plant sources were used for structural modification: corn, tapioca, and mung bean. The techniques employed for modification include enzymatic hydrolysis, freeze-drying, microprecipitation, and spray-drying.

Enzymes can depolymerize starch, converting it into simpler sugars, influenced by temperature and pH conditions. This process is crucial in the food industry to enhance starch functional properties, like solubility and viscosity. Additionally, they guarantee high selectivity and specificity under mild reaction conditions.(Zhong et al., 2022) Enzymatic hydrolysis takes advantage of α-amylase, which is an endoamylase that hydrolyzes the non-reducing ends of (1-4)-α-D-glucoside linkages in polysaccharides. Below the gelatinization temperature in a heterogeneous phase, where starch is dispersed in water, the enzyme creates surface holes in starch microparticles, adjustable by process parameters. Above this temperature, starch molecular weight is reduced, oligomers are produced, and viscosity is lowered. (Punia Bangar et al., 2022)

Lyophilization is a drying technique that involves the removal of a solvent, usually water, from a frozen sample through sublimation under vacuum conditions. This method is widely used in the food industry to produce isolates and extracts, ensuring strict thermal control to preserve heat-sensitive properties. During the lyophilization process, the sample is initially frozen at temperatures ranging from –30 to –50°C, and the water is subsequently removed as vapor without transitioning through

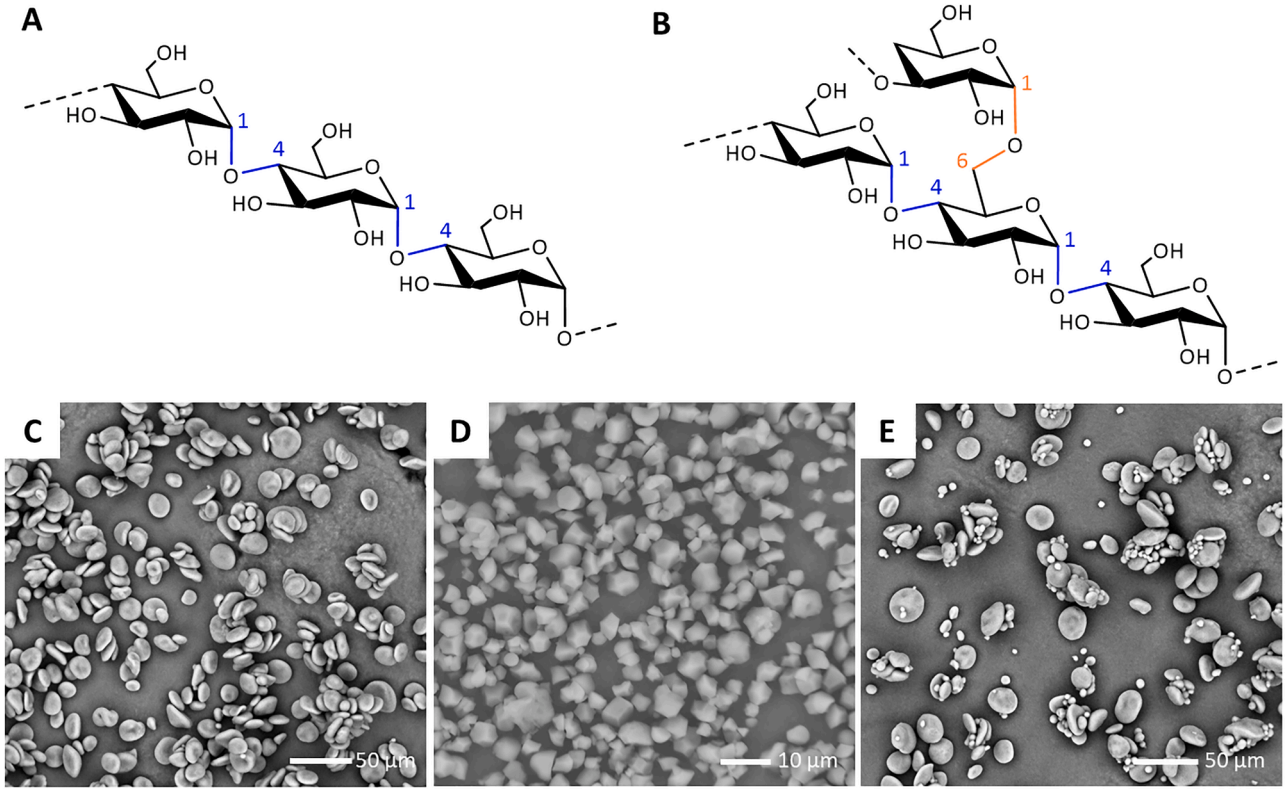


**Figure 1.** Structure and morphology of starches. A) chemical structure of amylose characterized by α(1-4) glycosidic bonds. B) chemical structure of amylose characterized by α(1-4) and α(1-6) glycosidic bonds. SEM images of barley, rice, and wheat starch granules (C, D, and E) are presented here solely for illustrative purposes to depict diverse native starch morphologies, whereas corn, tapioca, and mung bean starches were used for the experimental phases of this study.

the liquid phase. This approach is highly effective at preserving the structural integrity and organoleptic characteristics of materials, including thermolabile substances, thus maintaining the quality of the final product. (Abdelwahed et al., 2006; Ciurzyńska & Lenart, 2011; Mazár et al., 2025)

Spray-drying is a widely used drying method in the food and pharmaceutical industries, where a solution is atomized into droplets and rapidly dried in a heated chamber.(Patel et al., 2009; Thakur et al., 2024) With this technique, it is possible to micronize, dry powders, encapsulate, and change the material morphology.(Baltrusch et al., 2022) Controlling the drying rate, temperature, and material concentration influences the yield. Proper drying parameters are crucial for the desired outcome.

Starch morphologies from freeze-drying and spray-drying have diverse applications. Freeze-dried starches improve drug solubility (Liew et al., 2016) and stability in pharmaceuticals, (Pardeshi et al., 2023) while spray-dried, pre-gelatinized starches enhance food product stability. (Ma et al., 2022) However, these starch particles are not typically used to improve flowability or optical properties in formulations.

Based on these premises, the working hypothesis of this study was that the poor tactile aesthetics and grittiness of native starches, caused by their irregular and lamellar granular shapes, could be overcome by systematically restructuring their particle architecture. We hypothesized that transforming native corn, tapioca, and mung bean starches into controlled, smooth microparticles or specialized geometries (such as deflated spheres and donut-like structures) would successfully replicate the mechanical 'ball bearing' effect typical of synthetic microplastics. Specifically, it was hypothesized that these tailored morphologies would minimize skin friction and optimize powder flowability, thereby providing an eco-friendly and fully biodegradable texturizing alternative without compromising the sensory standards required for high-end cosmetic formulations.

Precipitation is an advanced technique for producing particles in the micrometer to nanometer range. Obtaining specific particle sizes and morphologies requires careful optimization of reagents and process parameters. In particular, the method and rate of introducing the starting material into the precipitation medium strongly influence nucleation and the controlled growth of microparticles. Optimizing these conditions enables the formation of particles with desired characteristics for specific applications. (Qin et al., 2016; Ulyarti et al., 2021)

With these techniques, we obtained various starch preparations of different morphologies, modulating physical properties such as size, surface adhesion, porosity, surface texture, and roughness. Additionally, we performed dye encapsulation to produce colored powders that are highly suitable for cosmetics, particularly for creating vibrant shades and subtle gradients in makeup. This process helped prevent diluting colors with white, which can cause duller tones. All components were plant-based, making the process fully sustainable and the final product biodegradable.

While comprehensive reviews, such as those by Punia Bangar et al. (2022) and Puri et al. (2025), have extensively documented the general chemistry, enzymatic hydrolysis, and broad industrial modifications of starches, they primarily focus on food or pharmaceutical macro-properties (e.g., solubility, viscosity, or thermal stability). A specific knowledge gap remains regarding how different botanical starch sources systematically respond to identical, established processing techniques (such as enzymatic erosion, microprecipitation, and spray-drying) when tailored exclusively for cosmetic-grade morphological control. The existing literature lacks a direct comparative framework that correlates structural variations across diverse starch origins (e.g., corn, tapioca, and mung bean) with key aesthetic and tactile parameters—such as skin friction, powder flowability, and the replication of the synthetic 'ball bearing' effect. This study directly addresses this gap by offering a systematic, side-by-side comparative analysis of these structural processing routes to provide precise morphological alternatives to microplastics.

Results indicate that these approaches can be applied to other types of starches and materials, providing a starting point to consider plant-based substances as promising alternatives, not only in cosmetics but also in food-edible and pharmaceutical fields. This study has the potential to guide the industry in rethinking the efficient use of natural components in formulations, allowing for the development of innovative products that align with market and environmental demands.

## 2. Materials and methods

Three distinct commercial-grade native starches were investigated in this study. Native corn starch (C*Gel 03401) was supplied by Cargill (Spain/Germany); according to the manufacturer's specifications, it consists of 100% *Zea mays* starch with a maximum moisture content of 14.0%, $\leq$ 0.4% d.b. protein, and ~0.1% ash. Native tapioca starch (TAPIOCA NATURAL, product code PDB 9096) derived from *Manihot esculenta* was manufactured by Agrana Starch (Austria) and distributed by A.D.E.A. S.r.l. (Italy), characterized by a moisture content $\leq$ 7.0% and ash $\leq$ 0.5%. Native mung bean starch (EXCELCARE MB) derived from *Vigna radiata* was purchased from SMS Corporation Co., Ltd. (Thailand), containing $\leq$ 13.0% moisture and $\leq$ 200 mg/kg sulfur dioxide. All starches were used as received without further chemical modification or laboratory extraction. Regarding the macromolecular features of the native botanical sources as described in literature, the typical amylose content is approximately 20–22% for corn starch (Krystyjan et al., 2022), 17–20% for tapioca starch (Zhu, 2015), and 30–35% for mung bean starch (Kaur et al., 2011; Min et al., 2026); and the average molecular weights generally range between $10^7$ and $10^8$ g/mol for amylopectin and $10^5$ and $10^6$ g/mol for amylose. Natural pigments were sourced from Aromata Group. Alpha-amylase, sodium phosphate dibasic and monobasic, tannic acid, and trehalose were purchased from Merck KGaA. Water used in all protocols was purified by passing through a MilliQ Millipore system. Ethanol and sodium chloride were sourced from CARLO ERBA Reagents S.r.l.

### 2.1. Protocol of enzymatic surface erosion

100 gr of native corn starch are dispersed in 100 mM phosphate saline buffer (PBS) with a concentration of 200 g $L^{-1}$. The solution is heated at 37°C under stirring. 0.6 gr of α-amylase are added, and the mixture is stirred for 24 h. To quench the reaction, 2.5 gr of tannic acid are added, and the solution is stirred for 30 min. The mixture is filtered and washed several times with water. The starch cake obtained is frozen at -80°C and freeze-dried.

### 2.2. Protocol of spray-dryer

10 gr of native corn or tapioca starch are dispersed in water to achieve a concentration of 100 g $L^{-1}$. After stirring for 1h, the solution is spray-dried. During this phase, other substances can be added to react with the sugar units of the starch. Spray-dry parameters are set as shown in Table S1. A dried powder is obtained from the collecting chamber. The spray-dryer used is a mini B-290 from BUCHI. The polymer must be solubilized in the solution, unless the morphology does not change. In the spray-dried solution, other substances such as sugars, organic acids, pigments, etc can be added.

### 2.3. Protocol of starch "sheets" synthesis

A solution of 100 g $L^{-1}$ is prepared with 10 gr of native corn starch dispersed in distilled water. The reaction is heated to 90°C and stirred under magnetic stirring for 1 h. Aside, 5.15 gr of trehalose are solubilized in distilled water with a concentration of 0.15 M. The mixture is poured into the starch solution and stirred at room temperature for 1h. The mixture is frozen at -80°C and freeze-dried. A white, crumbly block

is obtained. The solid is ground (with a ninja BN495 0,7000L blender) and micronized with a jet miller (injection pressure = 2.3 bar; ring pressure 2.3 bar).

Natural pigments or active ingredients can be added to the trehalose solution and poured into the starch solution and stirred at room temperature for 1h.

### 2.4. Protocol of starch "deflated spheres" synthesis

A solution of 75.2 g $L^{-1}$ is prepared with 10 gr of native corn starch dispersed in distilled water. The reaction is heated at 90°C for 1h under magnetic stirring to solubilize starch. The starch solution is poured into 133 mL of ethanol and stirred at room temperature for 1h. The reaction is filtered, frozen at -80°C, and freeze-dried. A white, crumbly block is obtained. The solid is ground and micronized with a jet miller (injection pressure = 2.3 bar; ring pressure 2.3 bar).

### 2.5. Protocol of starch "donuts" synthesis

The synthesis was adapted from the protocol described by Farrag et al.,(Farrag et al., 2018) with specific modifications. Initially, 16 gr of native corn or mung bean starch are dispersed in distilled water (53.3 g $L^{-1}$). The reaction is heated at 66°C under magnetic stirring for 1h. Ethanol (600 mL) is dropped in the starch solution, keeping a flow of 8 mL $min^{-1}$, and a second addition is repeated with a flow of 12 mL $min^{-1}$. The mixture is filtered, frozen at -80°C, and freeze-dried. A white product is formed. The solid is ground and micronized with a jet miller (injection pressure = 2.3 bar; ring pressure 2.3 bar).

### 2.6. Characterization

The morphology of the samples was analyzed using Phenom Pro Pure G6 Desktop scanning electron microscopy (SEM) – Thermo Fisher Scientific. Before analysis, the sample powder was loaded onto "MicroToNano" carbon tapes on a stub, and a vacuum was applied to remove impurities. Imaging was performed at accelerating voltages ranging from 5 to 15 kV, with various magnifications, and using the full Back-Scattered Detector (BSD) mode. Statistical analysis was carried out using ImageJ software, evaluating at least 100 particles across various magnifications and areas. This software enabled measurement of the Feret diameter (the distance between the two farthest points on the particle) and assessment of particle roundness. Attenuated Total Reflectance (ATR) spectroscopy measurements were carried out at room temperature using an Invenio® S FTIR Spectrometer (Bruker). Spectra were recorded in the range of 4000–400 $cm^{-1}$ in transmittance mode, with 128 scans and a resolution of 4 $cm^{-1}$. Powder X-ray Diffraction spectra (P-XRD) were collected with a MINIFLEX 600 HR. X-ray diffraction was performed with a monochromatic X-ray source (operating at 40 kV and 15 mA) and a D/teX Ultra 1D silicon strip detector. Data were recorded from 5° to 80° at a scanning speed of 5°/min. Using Origin software, it was possible to calculate the crystallinity index and percentage. The formulas used to calculate the crystallinity index (CI) and percentage (PC, using the two-phase method) are as follows:

$$CI = \frac{(I_{200} - I_{am})}{I_{200}} * 100$$

$$C(\%) = \frac{A_c}{A_c + A_{am}} * 100$$

The swelling power (SP) and water solubility index (WSI) of native and modified starch samples were determined in triplicate following a published method, (Ascheri et al., 2014) with minor modifications. Starch dispersions (2% w/w, dry basis, $D_S$) were prepared by adding distilled water to 1.0 gr of starch powder. The mixtures were heated at 80°C for 30 min under continuous stirring, cooled to room temperature, and subsequently centrifuged at 3000 rpm for 15 min. The supernatant was separated, transferred to an evaporating dish, and dried in an oven at 120°C for 4h. Both the wet sediment (swollen paste) and the dried supernatant solids were weighed. (Senanayake et al., 2013)

$$SP = \frac{weight\ of\ sedimental\ paste}{weight\ of\ the\ sample\ (dry\ basis)}$$

The Water Solubility Index (WSI) was calculated by weighing the dried starch and the starch obtained from the supernatant, using the following formula:

$$WSI = \frac{weight\ of\ dissolved\ solids}{original\ dry\ weight\ of\ starch} * 100$$

Thermal properties were investigated using Differential Scanning Calorimetry (DSC, TA Instruments, Trios software). A few milligrams of each sample were weighed into sealed aluminum crucibles, and measurements were performed between 25 and 200°C (instrument convention: Exo Down). The obtained thermograms were analyzed to determine the characteristic temperatures of the endothermic transition (onset, peak temperature, and endset), in order to evaluate the thermal behavior and stability of the material.

Viscosity is measured using an Anton Paar rheometer MCR 92 at controlled room temperature. Moisture content was determined using a Mettler Toledo HB43-S Halogen thermobalance. The powder was placed on an aluminium plate and heated to 160°C using the standard program, which involves a gradual increase in temperature. Microparticle size distribution was characterized using a Microtrac Sync analyzer, based on the volume percentage of the particles. The measurements were conducted with the "diffraction only" modality. The sample was placed directly into the dispersion chamber, and the analysis was repeated three times. Powder flowability was assessed by calculating the angle of repose. (Ravaghi et al., 2017; United States Pharmacopeia, 2024) The powder was poured into a funnel, the distances were recorded, and the angle was calculated using the following formula:

$$\theta = tan^{-1}\left(\frac{2h}{\overline{D}}\right)$$

For characterization of the tapioca starch nanoparticles, Nanoparticle Tracking Analysis (NTA) was performed. For cosmetic characterization, a specific rheometer for the powders was used: the Powder Flow Testing FT4 Rheometer. All analyses were performed using the standard protocols provided by the rheometer software.

The Oil Absorption Value (OAV) was determined using the spatula rub-out method in accordance with ASTM D281-12. (Maktabi et al., 2021) Briefly, 3.0 g of starch powder was weighed on a glass plate. Castor oil was added dropwise and thoroughly incorporated with a spatula until a homogeneous paste was formed without free powder particles. The OAV was calculated according to following formula:

$$OAV\ (\%) = \frac{\text{mass of absorbed oil (g)}}{\text{mass of dry powder (g)}} * 100$$

## 3. Results and discussion

Nowadays, synthetic alternatives such as polycaprolactone (PCL), (Christen & Vercesi, 2020) polyhydroxyalkanoates (PHA),(Choi & Choi, 2025; Sudesh et al., 2011) and polybutylene succinate (PBS)(Gan et al., 2023) are steadily increasing, employed in various applications, including formulations and packaging.(Giustra et al., 2024) However, it is appropriate to reconsider natural materials and renovate them to maximize their environmental compatibility, paving the way for truly sustainable solutions.

This research focuses on starches derived from three different plant sources, selected for their widespread availability and relevance across various regions worldwide. (Bertolini, 2010; Shoukat et al., 2025)

Corn, Mung bean, and Tapioca starches were modified by employing the following techniques: enzymatic hydrolysis, freeze-drying,

microprecipitation, and spray-drying. From the following results, we have discovered that the type of starch is crucial for the technique. Some protocols are ineffective for the morphological change. For instance, microprecipitation of tapioca starch leads to nanoparticles. Table 1 summarizes the principal information comparing the native starches to the modified ones.

### 3.1. Corn starch

Corn starch is an abundant biopolymer, and its derivatives are widely used in industrial applications, with 47.5% of starch products based on corn starch. In products, corn starch is used, such as in facial masks, (Suryani et al., 2022) for moisture absorption, flow enhancement, and bulking properties. (Ajayi & Amin, 2021)

In cold water, it is not soluble and forms a non-Newtonian fluid, a solution where particle-particle interactions within the liquid phase cause shear thickening.(Falana & Adenusi, 2026; Schneider & Gärtner, 2013) Dissolution of starch only occurs in hot water in an irreversible process called gelatinization.(Kulshreshtha et al., 2017) These physicochemical characteristics are closely related to the native granular structure of starch, in particular the ratio of amylose and amylopectin, and to possible morphological changes induced by processing or chemical modification.

Accordingly, scanning electron microscopy (SEM) was employed to investigate the morphological modification of the native corn starch (NCS) in treated samples, as shown in Figure 2 and Figure S1. NCS granules have an irregular shape: some are polygonal, while others are nearly spherical (Figure 2A). The chosen technique for starch treatment has a significant impact on the morphology of the microparticles. Enzymatic treatment does not alter the overall granular morphology; however, it induces the formation of holes and pores on the granule surface because of enzymatic activity (Figure 2B and Figure S2). These surface modifications may account for the improved smoothness observed in the treated particles, named ESE.

In contrast, morphological changes occur only when the polymer is first solubilized. In this case, starch loses its organized granular structure due to the disruption of hydrogen bonding interactions among amylose–amylose, amylose–amylopectin, and amylopectin–amylopectin chains. As a result, both spray-drying and microprecipitation processes yield deflated spherical particles.

During spray-drying, the rapid water evaporation from the polymer solution generates internal stresses, causing particle collapse and a characteristic deflated morphology (Fu et al., 2012) (Figure 2C and Figure S3). Notably, this structural outcome is observed for both corn and tapioca starch, indicating that the starch origin does not affect the final particle morphology under these processing conditions.

**Table 1**
Summary of the morphologies obtained by comparing the native starches to the modified ones.

| Technique | Starch | Morphology | Aspect | Flowability | Yield |
|---|---|---|---|---|---|
| Enzymatic hydrolysis | Corn | Smooth native-like, porous granules | White powder | Improved | 70-80% |
| Spray-drying | Corn | Deflated spheres | White powder | Worsened | 60-70% |
| Freeze-drying | Corn | Sheets | White powder | Worsened | 70-80% |
| Microprecipitation | Corn | Deflated spheres | White powder | Improved | 70-80% |
| Microprecipitation | Corn | Donuts | White powder | Worsened | 70-80% |
| Microprecipitation | Mung Bean | Donuts | White powder | Improved | 70-80% |
| Spray-drying | Tapioca | Deflated spheres | White powder | Worsened | 60-70% |

Precipitation results in the formation of two distinct shapes: deflated spheres and donut-like structures. The deflated spheres, produced via microprecipitation, are characterized by a collapsed morphology and a textured surface, as shown in Figure 2D. In contrast, donut-shaped particles are obtained through an aqueous-alcoholic treatment, a process that can be technically described as a form of anti-solvent-induced precipitation where ethanol reduces the solubility of the pre-swollen starch. Both morphologies feature a rough, lamellar surface—rather than external debris—formed by the leaching of peripheral amylose and subsequent structural shrinking. While most particles retain their overall integrity, the donut-shaped ones display a well-defined central cavity (Farrag et al., 2018) (Figure 2E and Figure S4).

In the microprecipitation process, the solvent addition rate plays a critical role in determining the final morphology. Deflated spheres are obtained when the antisolvent is added slowly to the polymer solution. In contrast, donut-shaped particles result when a larger volume of antisolvent is used, and the addition rate is even more controlled and slower. When the antisolvent is introduced, the polymer precipitates and undergoes structural reorganization. In the case of donuts, the slower addition rate likely allows the polymer to reorganize around the solvent, forming a central cavity. (Farrag et al., 2018) For deflated spheres, the antisolvent primarily surrounds the starch, resulting in the observed shape.

Microparticles produced by freeze-drying show sheet-like structures with a rough surface, indicating that the original shape is completely lost (Figure 2F and Figure S5). The loss of the morphology is due to the gelification of the starch. In this process, starch loses its crystalline structure and remains only the amorphous part. Once it is cooling starch reorganizes its structure in the “sheet” shape, probably due to the presence of water molecules. A similar morphological trend is observed for starch-based systems encapsulating pigments (Figure S6), which also form sheet-like structures upon freeze-drying. In this context, trehalose appears to play a key role, likely through the formation of hydrogen bonds with both starch and water, thereby promoting the development of extended sheet-like assemblies. Overall, the processing routes influence the morphology of the particles, leading to the formation of a wide range of structures. These differences in morphology are mainly associated with physical reorganization phenomena that occur during solubilization, precipitation, and drying of the starch backbone.

The statistical analysis of the Feret diameter reveals differences attributable to particle morphology (Figure 3). ESE most closely resembles native starch, which is expected since both have similar shapes; the only distinction is the slightly enzyme-eroded surface of ESE particles. For both NCS and ESE, the mean peak is around 11–12 μm, with a unimodal distribution. In contrast, the sheet-like particles display the greatest polydispersity and heterogeneity, likely due to their irregular shape. The distributions for deflated spheres and donut-shaped particles are asymmetric, which can be attributed to the presence of aggregates and incompletely precipitated particles formed during starch gelatinization. Spray-dried particles exhibit larger sizes, with a peak around 14 μm and a narrow distribution. Comparison of the histograms highlights how different treatments and morphologies can influence the Feret diameter.

Most of the samples exhibit a high roundness value (Figure 4), generally between 0.7 and 0.8, reflecting their morphology. As expected, the lowest roundness values are observed for the donut-shaped particles (0.62) and the sheets (0.54). This is predictable: the donuts have an elongated shape, while the sheets no longer possess a rounded morphology.

To verify that the applied treatments do not affect the chemical structure of starch, Fourier-transform infrared (FTIR) spectroscopy was carried out.

In Figure 5A, six IR spectra are compared: NCS, enzymatically treated starch, spray-dried particles, sheets, deflated spheres, and donut-shaped particles. All spectra display similar absorption bands, indicating that the treatments affect only the morphology of starch without altering

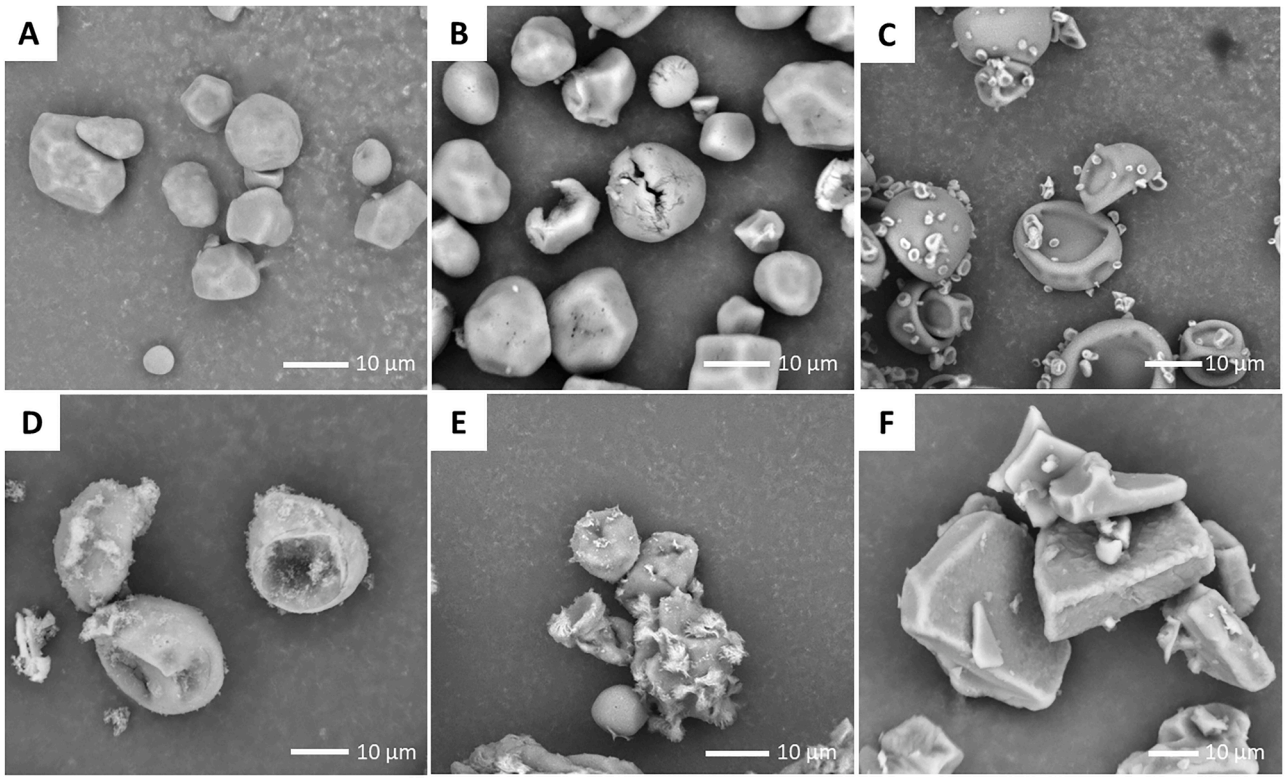


**Figure 2.** SEM images of different morphologies of corn starch. A) corn native starch B) Corn starch after enzymatic hydrolysis C) Spray-dried starch D) Deflated spheres. E) Donuts. F) Sheets.

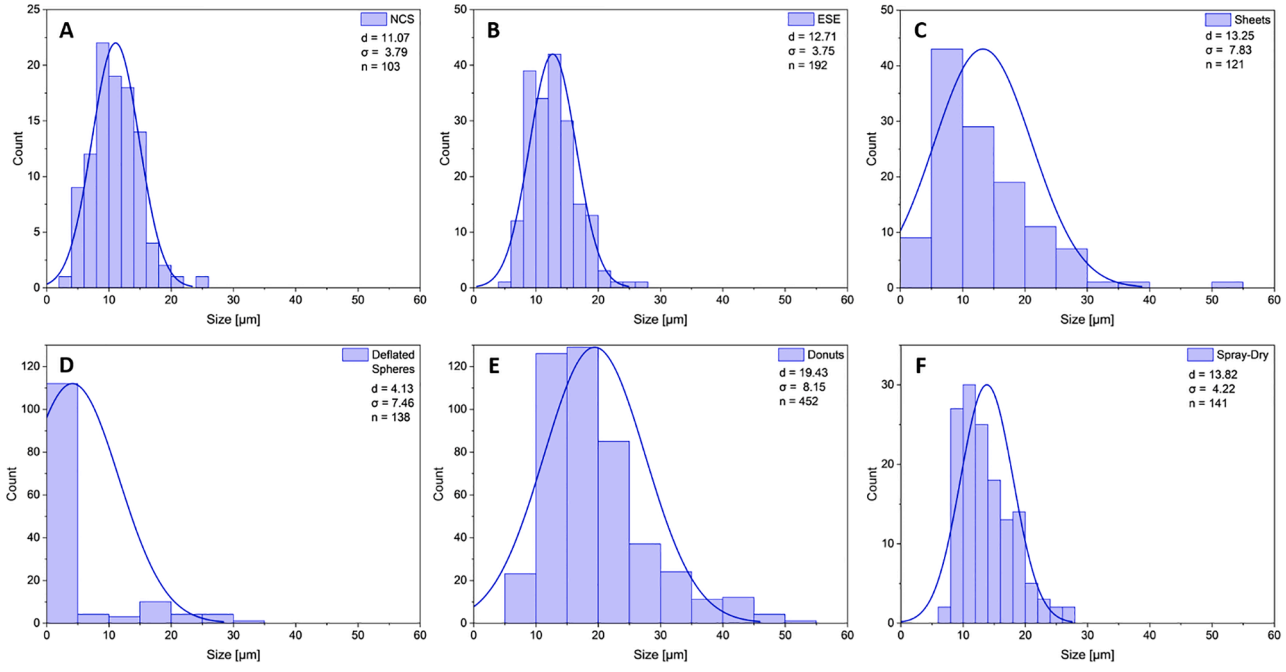


**Figure 3.** Statistical analysis of Feret diameter different morphologies of corn starch. A) corn native starch B) Corn starch after enzymatic hydrolysis C) Spray-dried starch D) Deflated spheres. E) Donuts. F) Sheets.

its chemical structure. The broad band at 3280 $cm^{-1}$ is linked to O-H stretching vibrations. The small peak at 2930 $cm^{-1}$ corresponds to aliphatic C-H stretching vibration. The band at 1640 $cm^{-1}$ is associated with the C-O bending of the OH group. The symmetric deformation and scissoring of $CH_2$ appear at 1430 $cm^{-1}$, and the symmetric bending of CH at 1360 $cm^{-1}$. At lower frequencies, the C-O-C asymmetric stretching appears at 1149 $cm^{-1}$, and C-O stretching occurs between 1100 and 990 $cm^{-1}$. The C-O-C ring vibration in carbohydrates shows three peaks at 928, 858, and 762 $cm^{-1}$. (Abdullah et al., 2018)

In Figure 5B, the spectrum of NCS is compared with that of the

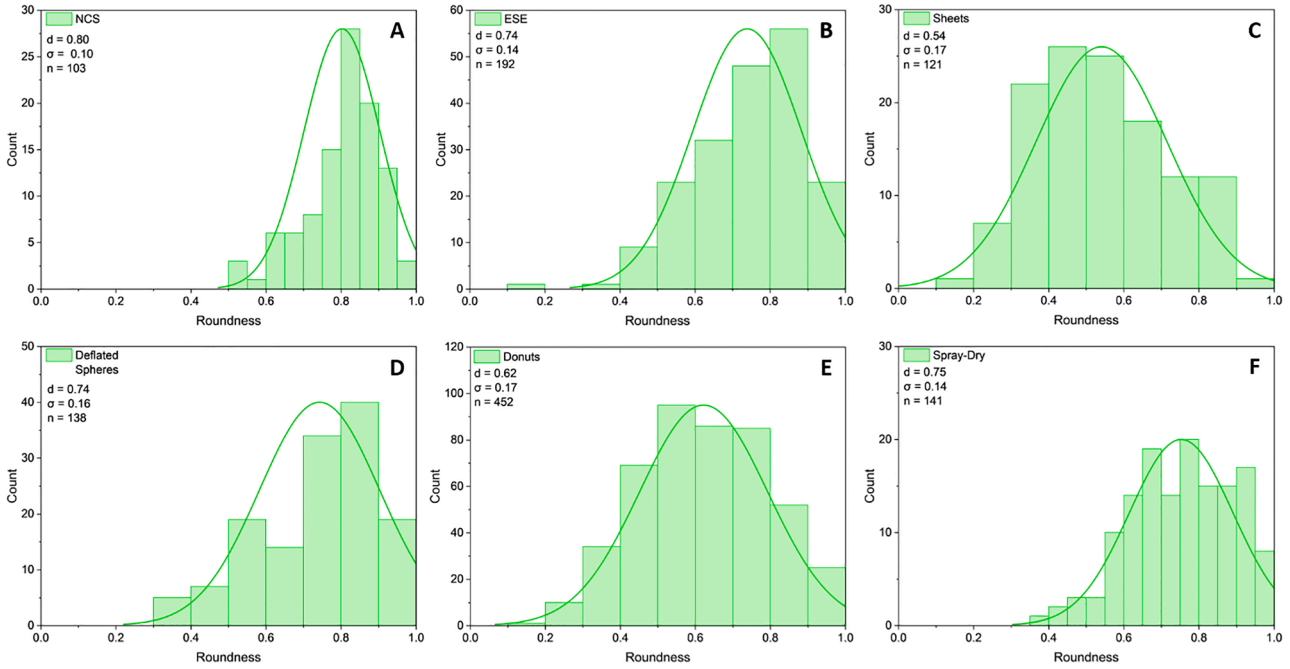


**Figure 4.** Statistical analysis of roundness of different morphologies of corn starch. A) NCS, B) ESE, C) Sheets, D) Deflated spheres, E) Donuts, F) Spray-dry.

colored sheets. The spectra show the same characteristic peaks, indicating that the incorporation of sugars does not alter the starch chemical structure. These FTIR results confirm that no new chemical bonds are formed, which is consistent with our objective of modifying starch morphology only.

The X-ray diffractogram of NCS shows four strong peaks at $2\theta = 15°$, 17°, 18°, and 23°, which are characteristic of the A-type crystalline structure. (Pozo et al., 2018) The diffractogram of the ESE sample is like that of NCS (Figure 5C), displaying the same four peaks associated with A-type crystallinity. This is expected, as enzymatic treatment occurs in an aqueous dispersion without solubilizing the starch, allowing the granules to retain their crystalline structure. The P-XRD spectra of the sheets, deflated spheres, donuts, and spray-dried corn starch (Figure 5D) are completely different from those of the NCS. The four peaks of the A-type structure disappear, leaving only a broad peak at around 18°. This suggests that the ordered structure of starch is lost and only the amorphous phase remains. This loss of crystallinity is further supported by the swelling behavior of the powder in water: the sheets absorb water instantly. (Ma et al., 2022) With a less organized structure, the starch chains can interact more readily with water through hydrogen bonding at room temperature, leading to rapid hydration.

The XRD spectra enabled a comparison of the crystallinity index (CI) and percentage crystallinity (PC). The NCS and ESE samples exhibit similar crystallinity values, confirming that they maintain a semi-crystalline structure (Table S2). In contrast, the other samples show CI and PC values of zero in the XRD spectra, indicating a loss of crystallinity and the formation of an amorphous material. Since the two-phase method was used, the software is unable to detect the small residual crystalline peaks, resulting in a value of zero. However, the actual crystallinity is likely to be around 1–5%.

It is important to acknowledge that while FTIR confirm the absence of synthetic chemical derivatization (ensuring a straightforward INCI regulatory status for cosmetic applications), the physical and enzymatic pathways evaluated here inherently alter the starch macromolecular architecture. Enzymatic erosion via $\alpha$-amylase cleaves glycosidic bonds (reducing molecular weight) while thermal processes like spray-drying disrupt the semi-crystalline granule framework. Although detailed chromatographic and rheological profiles (SEC/GPC, amylose/amylopectin ratio, and RVA pasting behavior) fell outside the analytical scope and timeframe of this cosmetic-focused study, future investigations incorporating these techniques are highly warranted to systematically map these internal macromolecular changes and precisely correlate them with the observed bulk functional properties.

The diffractometric analysis reveals that morphology affects the dimensions of the particles. All the powder samples have a high degree of polydispersity, with dimensions around 1 to 100 μm, except for the one treated enzymatically, which has particle dimensions between 1 and 40 μm (Figure 5E). NCS exhibits a unimodal particle size distribution with a mean of 20.15 ± 9.22 μm; however, the broad distribution indicates a high degree of polydispersity. ESE has a predominantly unimodal particle size distribution, with a major peak centred at 15.14 ± 4.03 μm. The powder with smaller dimensions is consistent with the enzyme erosion activity or hydrolysis.

A unimodal particle size distribution with a mean of 41.77 ± 13.81 μm and a broad distribution is also shown by deflated spheres. Same trend for donuts, which present a particle size of 28.39 ± 9.63 μm, exhibiting a high polydispersity. Deflated spheres and donuts are larger than starch, probably because they are swollen precipitated particles. Alternatively, it could be an effect of the solvent: ethanol may interact with the material (Figure 5E). The coloured and white sheets exhibit high polydispersity and have larger dimensions (Figure 5F). The solution was directly frozen without filtration, and then water was removed, which can lead to the formation of larger particles. It could also be due to the trehalose or the maltodextrins inside the pigments, which may interact with starch layers and make them more compact.

For most of the powders, the moisture content was above 10%, as shown in Table 2. In contrast, the moisture content of all the sheets was below 10%. While starch powders are generally bland, their moisture content can vary depending on morphology or the presence of encapsulated materials. Moreover, most of the powders exhibit poor flowability, with angles of repose above 30°. Exception for the ESE, which shows very good flowability with a parameter of 8.55° (Table 2). NCS, deflated spheres, and donut-shaped particles have an angle of repose of approximately 37°, while sheets display lower flowability, with angles around 44°, particularly when pigments are present.

These results indicate that morphology particle size alone does not determine flowability; rather, the workup and drying methods play a critical role. Powders that are precipitated, filtered, and washed tend to

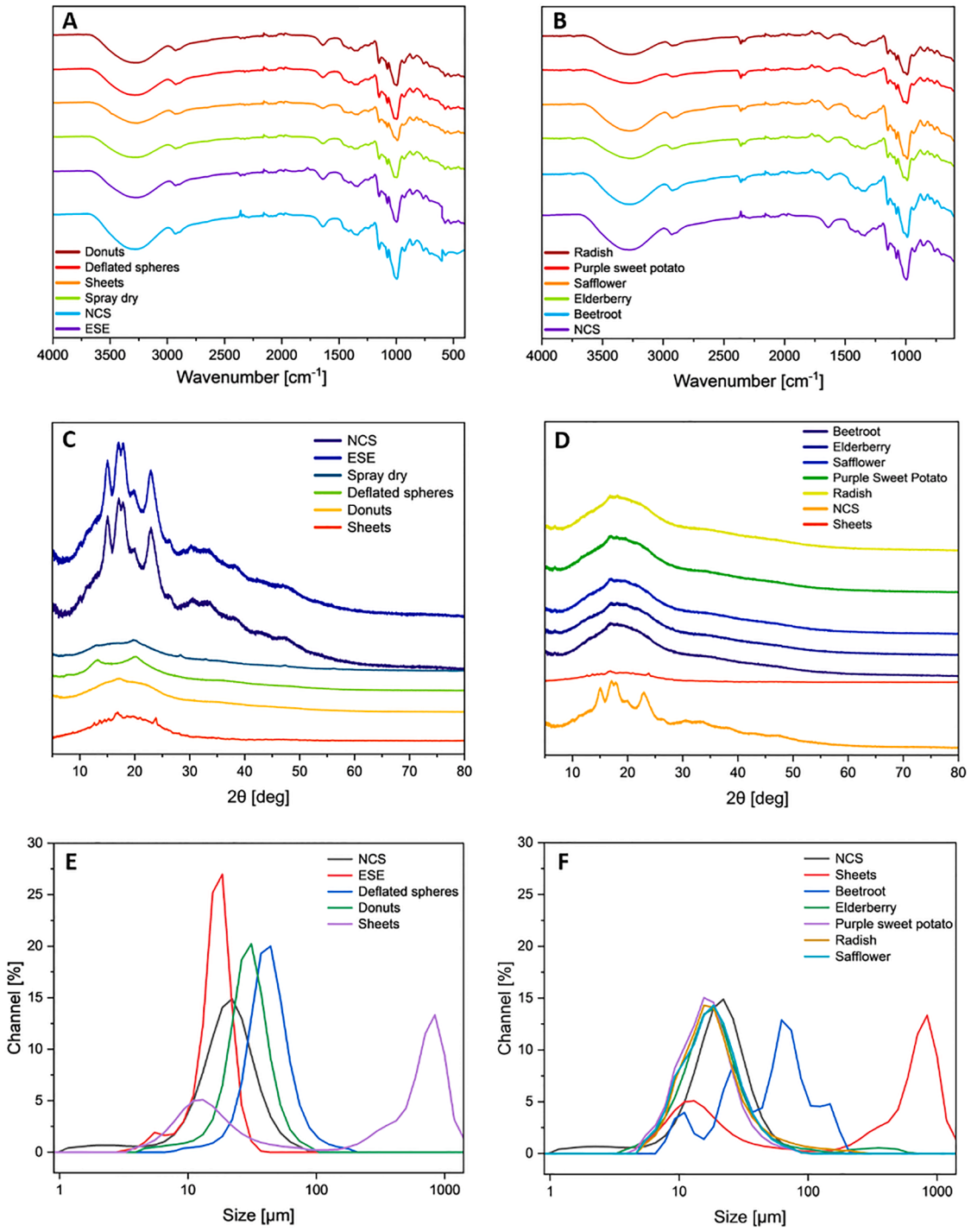


**Figure 5.** ATR spectra of different morphologies of corn starch: A) corn native starch compared with all the several morphologies; B) Corn starch compared with coloured sheets. PXRD spectra of different morphologies of corn starch: C) corn native starch compared with the one treated enzymatically; D) NCS and empty sheets starch compared with coloured sheets. Size distribution of different morphologies of corn starch: E) corn native starch compared with all the several morphologies; F) corn starch compared with uncolored and colored sheets.

have similar or improved flowability. Conversely, sheets, which do not undergo any additional processing, display worse flowability.

Spray-dried corn sample, despite being deflated spheres, demonstrates poor flowability, with an angle of 58.49°. Overall, among the tested methods, spray-drying yields the worst flow behavior, whereas enzymatic treatment produces the powder with the best flowability.

### *3.1.1. Swelling Power (SP) and Water Solubility Index (WSI)*

NCS exhibited a SP of 13.49 ± 1.96 g/g and a WSI of 12.01 ± 2.76%, values typical for untransformed native granules possessing balanced water hydration and restricted leaching of soluble polymers. ESE led to a slight increase in SP (14.95 ± 1.02 g/g) alongside a marked enhancement in WSI (32.97 ± 5.26%). This behavior indicates that α-amylase attack degraded amorphous granular domains, facilitating amylose diffusion into the aqueous phase while maintaining structural integrity. Donuts exhibited a high SP (18.28±4.53 g/g) with a moderate increase in solubility (WSI: 18.52 ± 2.81%), reflecting a network structure capable of retaining substantial water volumes without excessive

**Table 2**
Moisture content (MC%) and powder flowability of corn starch samples (NCS, ESE, spray-dried starch, deflated spheres, donuts and sheets) including corn-starch-based colored sheet (loaded with natural pigments: Beetroot, Elderberry, Safflower, Purple Sweet Potato, and Radish). Data represent mean ± SD (n = 3).

| Sample | MC(%) | Repose angle |
|---|---|---|
| NCS | 10.89 ± 0.18 | 37.61 ±3.62 |
| ESE | 11.52 ± 1.07 | 8.55 ± 0.55 |
| Spray-dry | 11.21 ± 0.63 | 58.49 ±1.66 |
| Deflated spheres | 10.34 ± 0.35 | 23.79 ±2.72 |
| Donuts | 13.00 ±0.61 | 36.77 ±2.81 |
| Sheets | 9.61 ± 0.27 | 38.88 ±1.92 |
| Beetroot | 7.05 ± 0.52 | 42.39 ± 1.39 |
| Elderberry | 8.89 ± 0.15 | 46.99 ± 1.97 |
| Safflower | 7.64 ± 0.17 | 47.60 ± 1.22 |
| Purple Sweet Potato | 8.57 ± 0.43 | 49.23 ± 5.34 |
| Radish | 7.64 ±0.42 | 55.96 ± 3.53 |

structural disintegration. Conversely, Deflated Spheres yielded the highest SP among all corn starch variants (23.20 ± 4.11 g/g) while maintaining a relatively low WSI (20.20 ± 1.89%). This indicates that microprecipitation enhanced structural porosity and polymer chain accessibility to water molecules without compromising inter-chain cohesion required to limit polymer leaching. From a formulation perspective, this combination represents the optimal performance for thickening and texturizing applications. On the other hand, Sheets showed a reduced SP (9.15 ± 2.06 g/g) combined with a high WSI (28.18 ± 2.34%), pointing toward structural rearrangements that constrained swelling while promoting polymer solubilization. Similarly, spray-dried corn starch displayed the lowest SP (8.78±1.26 g/g) and the highest overall solubility (35.64 ± 9.26%). This behavior confirms that thermal atomization disrupted the native granular architecture, leading to predominant solubilization over controlled hydration.

### 3.1.2. *Thermal properties (DSC)*

Differential Scanning Calorimetry was employed to complement the structural characterization of corn starch samples. All samples display a broad endothermic transition (Exo Down convention), attributable to gelatinization and the progressive loss of crystalline order of starch (Figure S7). NCS shows a broad, symmetric transition between 95 and 100°C (Endset = 169.4°C), consistent with its semicrystalline A-type structure. ESE exhibits a similar broad peak between 90 and 95°C, with slightly lower intensity and an Endset of 173.1°C, in agreement with its largely preserved crystallinity.

The Deflated Spheres sample shows a broad transition over an extended temperature range (95–100°C), consistent with a heterogeneous structure. Donuts presents a broad peak shifted to higher temperature (105–110°C), the highest transition temperature among the corn samples, indicating that more energy is required to complete the transition and pointing to a more thermally stable or constrained structure. The Sheets sample (90–95°C) shows a small secondary peak around 105°C, indicating a two-step transition consistent with the presence of multiple crystalline populations or a recrystallized fraction, in line with the loss of the A-type crystalline pattern discussed above. The Spray-dried sample shows the narrowest transition and the lowest peak temperature (75–80°C, Endset = 128.4°C), consistent with its lower crystallinity and more homogeneous, amorphous population of particles. Data are summarized in Table 3.

**Table 3**
DSC thermal characterization of corn starch samples.

| Sample | Peak (°C, range) | Shoulder/ 2nd peak (°C) | Endset (°C) | Observations |
|---|---|---|---|---|
| NCS | 95 – 100 | - | 169.4 | Broad, symmetric transition; moderate crystallinity |
| ESE | 90 – 95 | - | 173.1 | Broad peak, slightly lower intensity than NCS |
| Deflated Spheres | 95 – 100 | - | n.d.* | Broad transition over an extended range; heterogeneous structure |
| Donuts | 105 – 110 | - | n.d.* | Shifted to higher T; more stable/constrained structure (highest transition T among corn samples) |
| Sheets | 90 – 95 | ~105 (shoulder) | n.d.* | Two-step transition; multiple crystalline populations or a recrystallized fraction |
| Spray-dried | 75 – 80 | - | 128.4 | Narrow transition; lowest T and sharpest peak among corn samples, lower crystallinity |

* n.d. = endset not automatically extracted by the software from the available thermogram.

## 3.2. *Mung bean starch*

Starch is the most common carbohydrate in seeds (22-45%). Legume starches play a key role in some sectors: mung bean (*Vigna radiata*) starch is reported as the best material for noodle preparation in the food industry. (Hoover et al., 1997) whereas modified, cross-linked mung bean starches are used in pharmaceutics as gelling agents and emulsion stabilizers. (Kittipongpatana & Kittipongpatana, 2015; Ma et al., 2025)

To better understand how these functional properties relate to particle structure, the morphology of native and processed mung bean starch was examined using SEM.

SEM images comparing native mung bean starch (NMS) and donut-shaped (DMS) particles are shown in Figure 6A. NMS granules appear rounded with a smooth surface and display a heterogeneous size distribution. Following microprecipitation, not all particles assume the donut shape; instead, three distinct morphologies can be observed. The first type has completely lost its original structure, appearing flat with irregular or indented edges. The second type exhibits a donut-like shape with a smooth surface and a central hole (Figure 6B and C). The third type closely resembles NMS.

For corn starch, statistical analysis of the Feret diameter reveals differences attributable to particle morphology (Figure 7). The distribution for the donut-shaped particles is broader and more polydisperse compared to native starch. This can be explained by the more elongated shape of the donut particles relative to the starting material, as well as the presence of some particles that did not reorganize properly during precipitation, resulting in irregular morphologies.

Both samples exhibit a moderate roundness value of approximately 0.63, which reflects their elongated morphology. This is likely because both NMS and DMS possess an elongated shape.

The NMS and DMS samples exhibit similar crystallinity values, confirming that they retain a semicrystalline structure (Table S2). The Donut samples display a crystallinity index (CI) of 55.84%, while the percentage crystallinity (PC) is 34.43%. This discrepancy is likely due to the different calculation methods used. The CI, which is based on the ratio between the intensity of the crystalline and amorphous peaks, is more sensitive to peak shape and intensity. In contrast, the PC provides a more quantitative assessment, as it considers the total area under the peaks.

These observations suggest that the current treatment is not strong enough to uniformly alter the morphology of all particles. Alternatively, adjusting the process parameters could be explored to favor the formation of a specific particle shape.

As already mentioned above, the polymer precipitates and reorganizes thanks to the lower addition of the solvent, leading to a central cavity. Probably not all the microparticles have time to reorganize because they are flat.

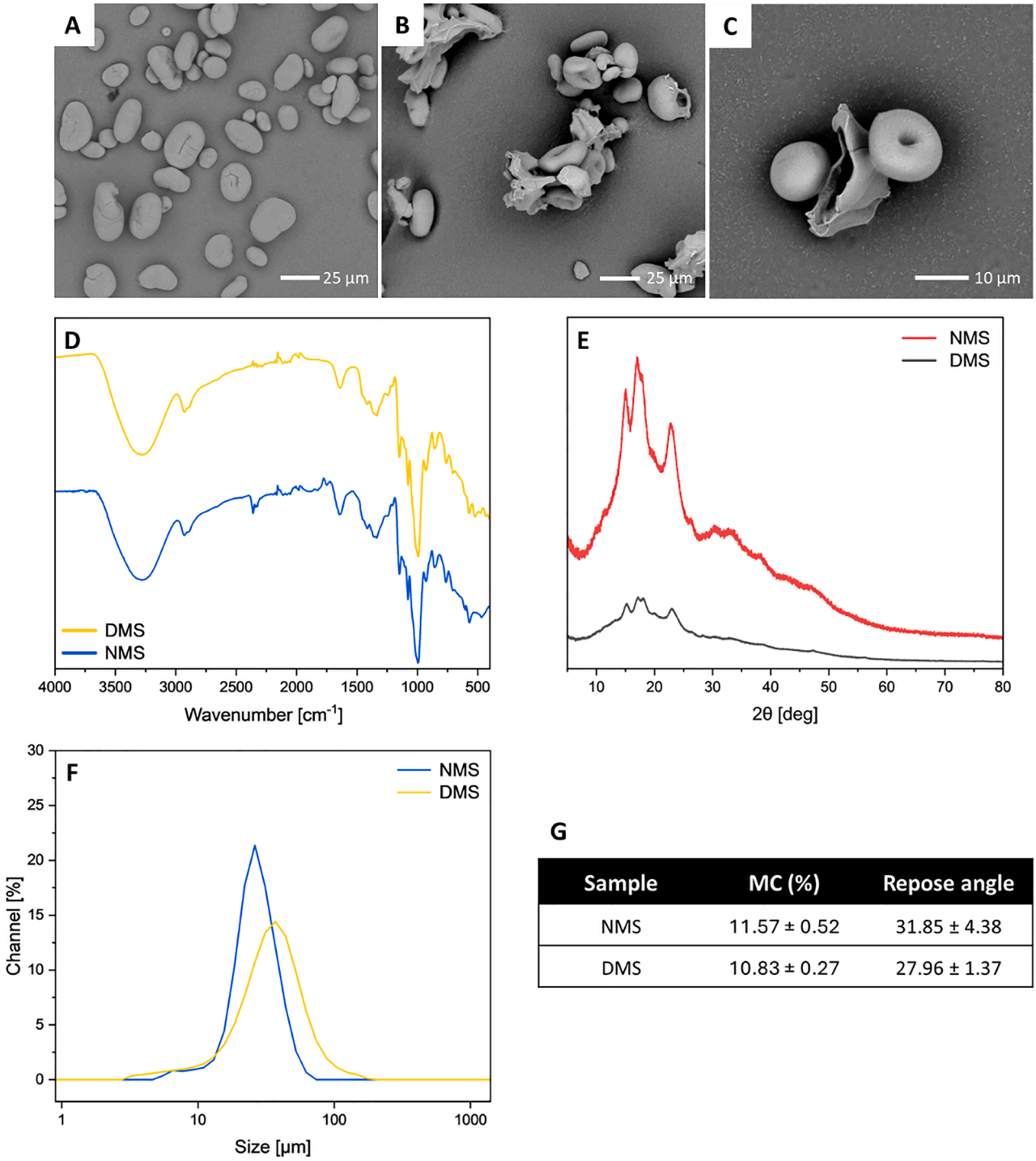


G

| Sample | MC (%) | Repose angle |
|---|---|---|
| NMS | 11.57 ± 0.52 | 31.85 ± 4.38 |
| DMS | 10.83 ± 0.27 | 27.96 ± 1.37 |

**Figure 6.** SEM images of different morphologies of Mung Bean starch: A) NMS; B) DMS; C) DMS (higher magnification). D) ATR spectra of NMS and DMS. E) XRD spectra of NMS and DMS. F) Size distribution of NMS and Donuts. G) Moisture content and powder flowability of NMS and DMS. Data represent mean ± SD (n = 3).

In Figure 6D, two FTIR spectra are compared: NMS and DMS particles. Both spectra display the same characteristic peaks observed for corn and tapioca starches, confirming that no chemical bonds are formed and that only the particle morphology is modified.

The X-ray diffractogram of NMS shows the same structure as the other native starches (Figure 6E). The XRD spectrum of mung bean donuts closely resembles that of native starch, indicating that under this type of treatment, which involves an aqueous-alcoholic treatment without starch solubilization at 90°C, the crystalline structure is largely preserved.NMS and DMS powders have particle sizes ranging from 5 to 100 µm and exhibit a unimodal distribution (Figure 6F), with average sizes of 25.04 ± 8.21 µm and 34.90 ± 16.09 µm, respectively. However, the broad size range indicates a high degree of polydispersity.

They had moisture content above 10% (Figure 6G). The slightly lower moisture observed in donuts is likely due to processing: filtration and freeze-drying remove water and other compounds, producing a denser powder. Both NMS and DMS exhibit poor flowability, with values respectively of 31.85° and 27.96°. As already noted for moisture content, the work-up is crucial for the powder compactness, justifying the lower value of the repose angle of the donuts.

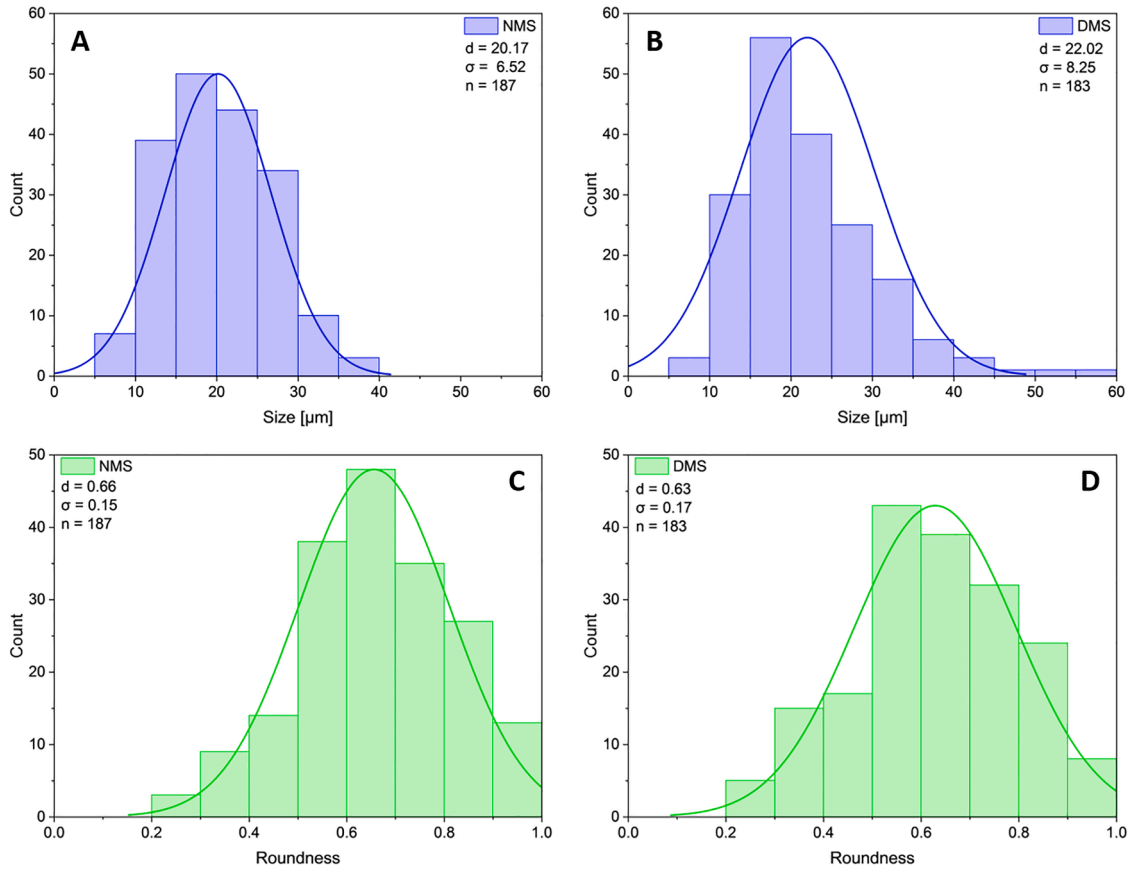


**Figure 7.** Statistical analysis of Feret diameter: A) NMS, B) DMS; and roundness: C) NMS, E) DMS.

### 3.2.1. *Swelling Power (SP) and Water Solubility Index (WSI)*

NMS displayed a high SP (14.10 ± 0.21 g/g) and a moderate WSI (17.61 ± 0.03%), reflecting effective granule hydration. For DMS, both parameters dropped (SP: 8.52 ± 0.76; WSI: 5.53 ± 1.10%). This dual reduction suggests that the aqueous-alcoholic treatment promoted a denser, highly packed polymer assembly that resisted water penetration and suppressed amylose leaching. Consequently, DMS offers functional potential for formulations demanding high thermal stability and resistance to granule disintegration.

### 3.2.2. *Thermal properties (DSC)*

Both mung bean samples show a broad endothermic peak, attributable to gelatinization and the progressive loss of crystalline order. In NMS, the transition ends at approximately 161.9°C, with a peak maximum around 90°C. In DMS the endothermic peak is shifted to higher temperature, with a maximum around 110–120°C and an Endset of 189.3°C. This behavior suggests that the aqueous-alcoholic processing treatment modifies the starch structure, requiring a greater amount of energy to complete the thermal transition, consistent with the CI/PC data (Table S2), which indicate that DMS retains a semicrystalline structure. The increase in the final transition temperature may be associated with reorganization of the polymer chains during processing, stronger intermolecular interactions, and a reduction in molecular mobility due to the formation of a more compact structure. Data are summarized in Table 4.

**Table 4**
DSC thermal characterization of mung bean starch samples.

| Sample | Peak (°C, range) | Endset (°C) | Observations |
|---|---|---|---|
| NMS | ~90 | 161.9 | Typical gelatinization behavior of native starch |
| DMS | 110 – 120 | 189.3 | Markedly higher Endset: processing treatment modifies the structure, requiring more energy to complete the transition |

### 3.3. *Tapioca starch*

"Tapioca" refers to the starch sourced from or other processed products made from the cassava plant. (Hsieh et al., 2019) More specifically, tapioca starch is produced by pre-hydrating cassava roots, and it is less granular than corn starch. It can be found in cosmetic products because of its properties like gelatinization, increased stability, and sensory benefits improvement. (Infante et al., 2024) Furthermore, owing to its lower viscosity compared to the other starches tested, it was identified as a promising polysaccharide candidate for spray-drying applications. To better understand how these properties relate to particle structure, the morphology of native and processed tapioca starch was examined using SEM.

The SEM images of native tapioca starch (NTS) and spray-dried samples are shown in Figure 8A-C. NTS granules are semi-spherical with a smooth surface. Spray-dried tapioca starch (TSD) exhibits a different morphology compared to the NTS granules; however, the original semi-spherical shape is largely retained. The microparticles appear deflated on one or more sides and show size variation. Additionally, Spray-dried tapioca starch microparticles containing trehalose (TSDT) exhibit a similar morphology, although they are not identical. Their shape is a deflated sphere with a smooth surface, and their sizes are not uniform. Some microparticles seem more deflated on one side while remaining swollen on the other.

The Feret diameter of NTS is similar to that of the spray-dried samples (TSD and TSDT) (Figure 9). Samples display a sharp peak, with a mean value around 13 μm. This similarity can be attributed to the fact

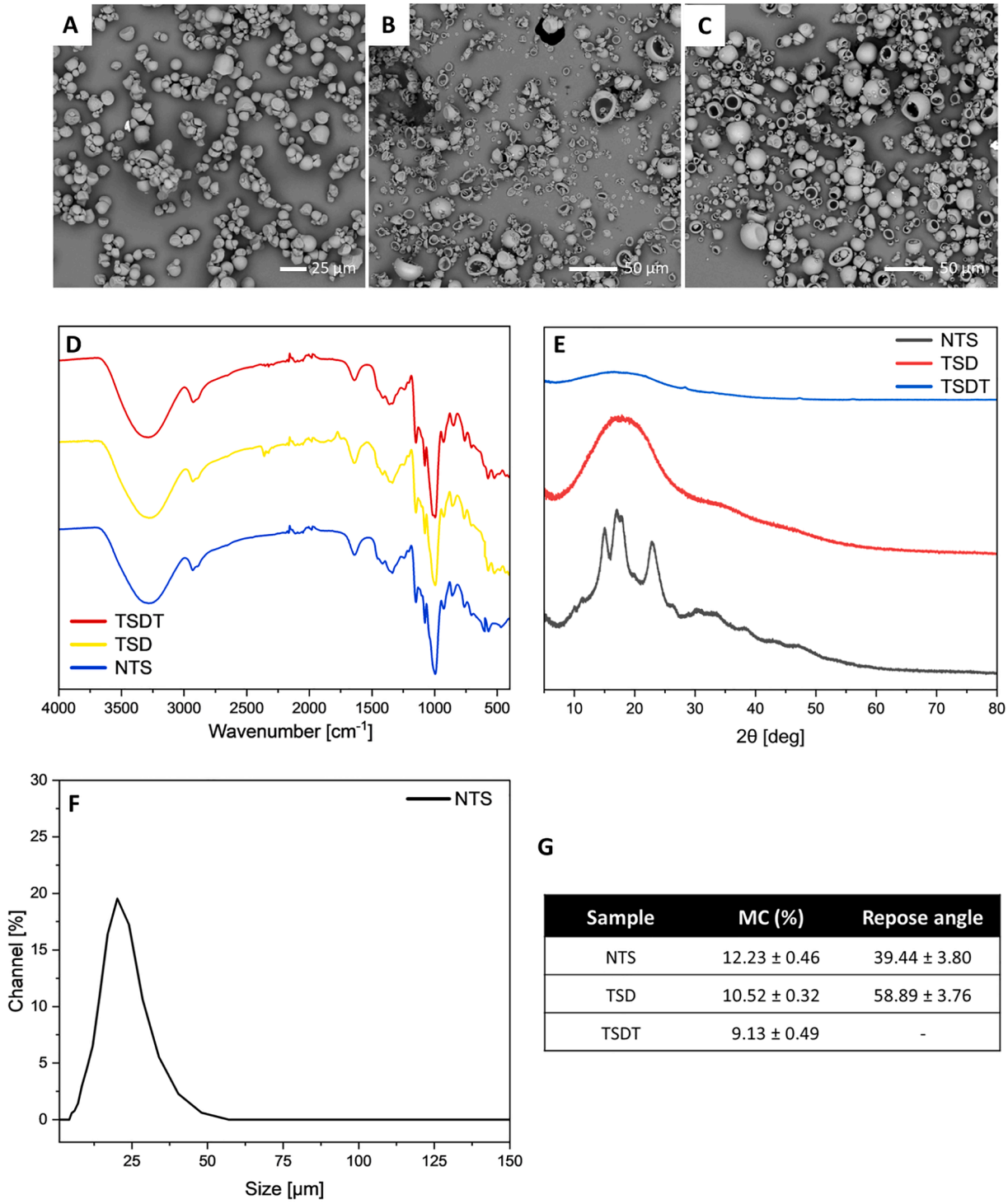


| Sample | MC (%) | Repose angle |
|---|---|---|
| NTS | 12.23 ± 0.46 | 39.44 ± 3.80 |
| TSD | 10.52 ± 0.32 | 58.89 ± 3.76 |
| TSDT | 9.13 ± 0.49 | - |

**Figure 8.** SEM images of different morphologies of Tapioca starch: A) NTS; B) TSD; C) TSDT. D) ATR spectra of NTS, TSD, and TSDT. E) XRD spectra of different morphologies of NTS, TSD, and TSDT. F) Size distribution of NTS. G) Moisture content and powder flowability of NTS, TSD, and TSDT. Data represent mean ± SD (n = 3).

that their morphology remains largely unchanged; the particles retain their rounded shape and are simply deflated following the spray-drying process. Moreover, all the samples exhibit a high roundness value of approximately 0.72, which is consistent with the findings for the Feret diameter.

As already mentioned, during spray-drying, the polymer solution is dried very rapidly, resulting in the quick evaporation of the solvent, which leads to deflated spheres.

In Figure 8D, three FTIR spectra are compared: NTS, TSD, and TSDT. All three tapioca starch spectra resemble those of corn starch, showing similar features, and confirming that the treatments induce only morphological, not chemical, changes. NTS exhibits the same characteristic absorption bands observed for corn starch, including the O–H stretching at 3280 $cm^{-1}$, aliphatic C–H stretching at ~2930 $cm^{-1}$, $CH_2$ deformation bands at 1430 and 1360 $cm^{-1}$, and the typical carbohydrate-related C–O and C–O–C vibrations in the 1150–990 $cm^{-1}$

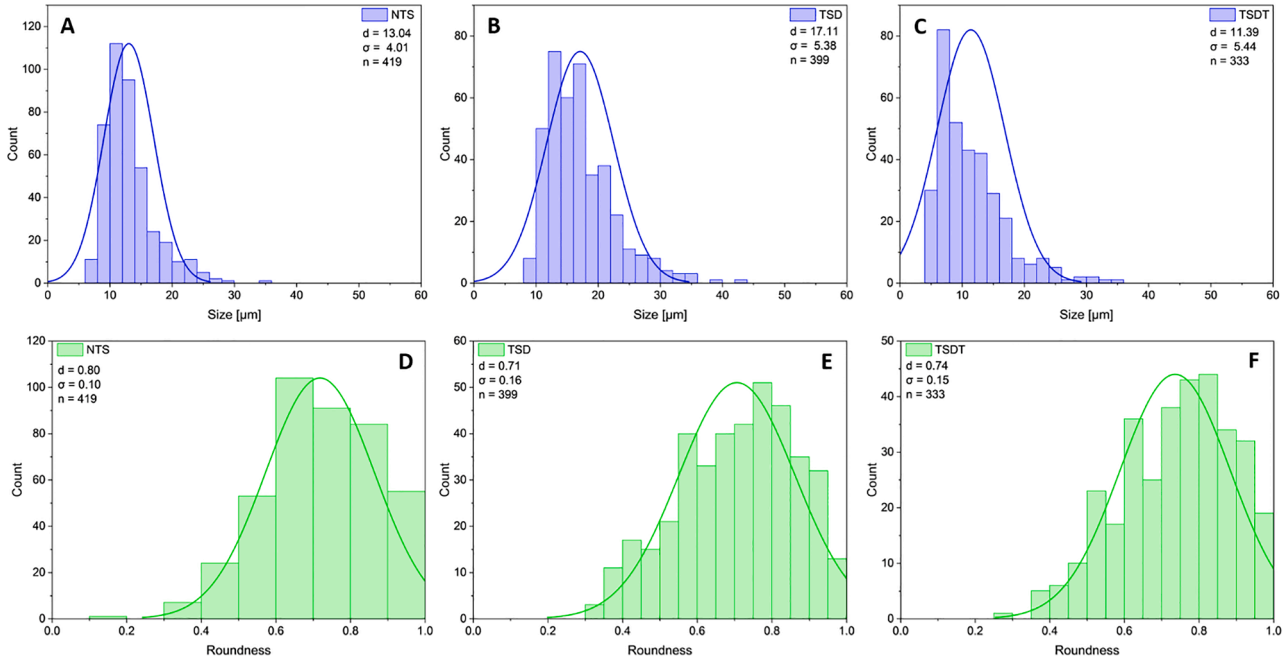


**Figure 9.** Statistical analysis of Feret diameter: A) NTS, B) TSD and C) TSDT; and roundness: D) NTS, E) TSD and F) TSDT.

region. The fingerprint region (928, 858, and 762 $cm^{-1}$) further confirms the presence of the polysaccharide ring structure. (Abdullah et al., 2018)

The X-ray diffractogram (Figure 8E) of NTS shows four strong peaks at $2\theta = 15°$, 17°, 18°, and 23°, which are characteristic of the A-type crystalline structure. (Pozo et al., 2018) Spray-drying results in the loss of A-type crystallinity because the four peaks disappear, leaving one broad peak at 18°, indicating that only the amorphous part remains. The diffractometric analysis can only be performed on NTS. The spray-dried samples swell immediately when wet with water. NTS ranges in size from 5 to 80 μm and shows a unimodal particle size distribution with an average of 19.56 ± 6.73 μm; however, the broad distribution suggests a high level of polydispersity.

Native tapioca starch exhibits higher crystallinity compared to the other two starches and displays a clear semicrystalline structure (Table S2). In contrast, the modified corn starch samples have CI and PC values equal to zero, indicating a loss of crystallinity and the formation of an amorphous material. However, this zero value may reflect a limitation of the instrument in detecting any residual crystalline regions that may still be present.

For the powders, both NTS and the TSD exhibit moisture contents above 10%, as reported in Figure 8G. Instead, TSDT has a moisture content below 10%, suggesting that the presence of sugar can also influence water retention. Trehalose has several hydroxyl groups that can form hydrogen bonds with starch, which may contribute to better powder compactness and reduced humidity.

All the powders present poor flowability, with values respectively of 39.44° for the untreated and 58.89° for the spray-dried sample (Figure 8G). This indicates that the spray-drying process negatively affects powder flow properties.

As already stated, the typology of starch is critical in the

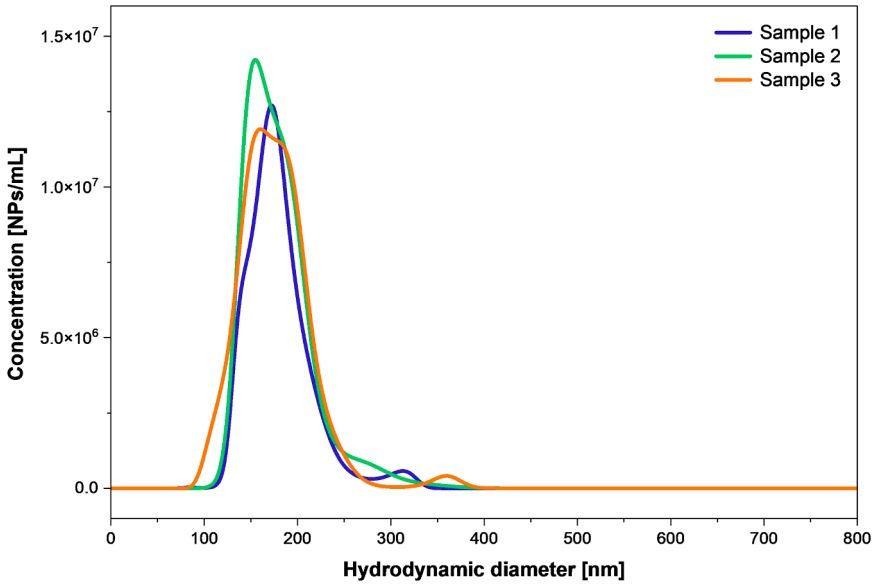


**Figure 10.** Nanoparticle tracking analyzer of tapioca starch nanoparticles.

rearrangement of amylose and amylopectin, which determines the resulting particle morphology. Both the deflated sphere and donut protocols were tested, leading to the formation of nanoparticles. The samples are highly polydisperse and exhibit a multimodal size distribution. A population of particles has dimensions below 100 nm, as indicated by the sharp peak, while the overall particle size ranges from 20 to 450 nm (Figure 10).

However, due to their small size, these nanoparticles are not suitable for cosmetic applications, as they may penetrate the skin. Instead, this ability to penetrate biological barriers makes them highly valuable for biomedical applications, particularly in targeted drug delivery and therapeutic systems. In contrast, the larger microparticles described earlier, including deflated spheres, donuts, and sheets, are within a safe size range and retain the desired morphology, making them more suitable for cosmetic formulations.

#### 3.3.1. Swelling Power (SP) and Water Solubility Index (WSI)

NTS showed a low SP (4.53 ± 0.94 g/g) accompanied by a very high WSI (63.26 ± 6.20 %), indicating that native granules readily solubilize upon heating rather than swelling intact. TSD enhanced water absorption, elevating SP to 11.54 ± 1.35 g/g (a ~2.5-fold increase over NTS) while reducing WSI to 39.57 ± 2.23%. This structural transformation rendered the amorphous matrix accessible to water while preserving sufficient matrix integrity. For TSDT, SP remained virtually unchanged (11.51 ± 1.96 g/g), whereas WSI rose to 67.49 ± 6.53%. The elevated "WSI is directly attributable to the dissolution of the co-formulated sugar fraction. Functionally, TSD is ideal for cosmetic systems requiring high viscosity and granule stability, whereas TSDT is advantageous for fast-dissolving or instant dispersible formulations.

#### 3.3.2. Thermal properties (DSC)

NTS displays a broad thermal transition at 110–115°C, indicative of moderate crystallinity, in agreement with the P-XRD data showing that NTS retains the highest crystallinity among the tapioca samples (Table S2). TSD shows the lowest and broadest gelatinization/melting transition, between 70 and 80°C, suggesting partial disruption of starch crystallinity during spray-drying, consistent with the loss of the A-type diffraction pattern discussed above. TSDT exhibits a broad peak between 100 and 105°C, with greater energy absorbed during gelatinization, likely due to the influence of the sugar on the transition and in line with the lower moisture content measured for this sample. Data are summarized in Table 5 obtained from Figure S9.

### 3.4. Oil absorption capacity of modified starches

A crucial functional property for powders intended for cosmetic applications is the Oil Absorption Value (OAV), which reflects the ability of the material to absorb lipids and contributes to skin-feel, mattifying power, and formulation stability. The OAV was evaluated using castor oil according to the standard spatula rub-out method (ASTM D281-12). (Maktabi et al., 2021) As reported in Table S3, a clear correlation emerges between the crystalline status/morphology of the powders and their lipid absorption capability:

**Table 5**
DSC thermal characterization of tapioca starch samples.

| Sample | Peak (°C, range) | Endset (°C) | Observations |
|---|---|---|---|
| NTS | 110 – 115 | n.d.* | Moderate crystallinity |
| TSD | 70 – 80 | n.d.* | Lower, broad transition; partial disruption of crystallinity during spray-drying |
| TSDT | 100 – 105 | n.d.* | Greater energy absorbed during gelatinization, likely due to the influence of the sugar on the transition |

* n.d. = endset not automatically extracted by the software from the available thermogram.

*Corn Starch*: NCS and ESE retained their crystalline structure (CI = 36.86% and 35.68%, respectively; Table S2) and displayed lower OAVs of 33.41% and 31.06%. In contrast, completely amorphous, spray-dried structures (Table S2) exhibited higher values. Specifically, Sheet-shaped (93.40%) and Deflated Spheres (86.56%) starches showed the highest oil retention capabilities, followed by Donuts (53.63%) and Spray-dry (53.36%).

*Mung Bean Starch*: NMS (CI = 35.99%) exhibited an OAV of 25.58%. Upon DMS, which altered the crystalline arrangement (Table S2), the OAV more than doubled to 60.05%.

*Tapioca Starch*: A similar trend was observed for tapioca starch. NTS (CI = 40.92%) showed an OAV of 34.35%, whereas spray-dried samples displayed increases, reaching 55.77% for TSD and 85.06% for TSDT. Across all starch botanical origins, an interesting and consistent pattern is observed: samples maintaining a semi-crystalline granules structure display modest oil absorption, whereas spray-dried amorphous forms exhibit substantially higher OAVs. This behavior can be attributed to both microstructural and physical characteristics. The loss of long-range crystalline order, combined with the porous, hollow, or irregular geometries produced during spray-drying, increases the specific surface area and structural porosity, allowing oil to penetrate and be retained more effectively. Additionally, the fluffier, low-density nature of the amorphous powders increases capillary uptake and mechanical resistance during paste formation.

### 3.5. Rheological characterization and potential for cosmetic applications

To evaluate the potential of ESE as a functional ingredient, its mechanical and rheological behavior was assessed, simulating the conditions required for integration into cosmetic matrices such as face powders, bronzers, and blushes. The powder samples were characterized via rheometric analysis to determine their suitability for industrial handling and application. Compressibility tests were performed to quantify the densification potential of the formulations under vertical stress (Figure S11), while shear tests were employed to assess flowability and internal friction parameters (Figure S12), which are critical for ensuring product performance and application consistency. Data are summarized in Table 6 and 7.

The Conditioned Bulk Density (CBD) of the NCS sample, which characterizes the material density following the displacement of interstitial air, was found to be marginally higher than that of the enzymatic powder (ESE). This disparity suggests that NCS possesses a higher intrinsic density and superior compactability. Furthermore, the compressibility percentage was measured at a normal stress of 15 kPa to quantify the volumetric reduction under mechanical load (Figure S11). The NCS sample exhibited higher compressibility than ESE; this behavior is likely attributable to the initial packing state of the enzymatic powder, which suggests a more stable, pre-packed configuration that limits further densification.

Cohesion was evaluated to quantify the interparticle attractive forces in the absence of external consolidating pressure. The NCS sample exhibited higher cohesion compared to ESE, indicating a pronounced propensity for agglomeration. This trend was further corroborated by the Unconfined Yield Strength (UYS); the higher UYS values recorded for NCS indicate that greater stress is required to initiate flow in the consolidated material, confirming a higher risk of obstruction formation. The Major Principal Stress (MPS), representing the maximum consolidating stress applied before flow resistance assessment, remained

**Table 6**
Compressibility test results.

| Sample | CBD (g $mL^{-1}$) | CPS (%) - 15 kPa |
|---|---|---|
| NCS | 0.642 | 9.76 |
| ESE | 0.614 | 7.66 |

*CBD (Conditioned Bulk Density), CPS (Compressibility percentage)

**Table 7**
Shear cell results.

| Sample | Cohesion (kPa) | UYS (kPa) | MPS (kPa) | FFc | AIF (°) | BD (g $mL^{-1}$) |
|---|---|---|---|---|---|---|
| NCS | 0.373 | 1.26 | 9.50 | 7.51 | 29.0 | 0.630 |
| ESE | 0.294 | 0.997 | 9.36 | 9.39 | 28.9 | 0.250 |

*UYS (Unconfined Yield Strength), MPS (Major Principal Stress), FFc (Flow Function Coefficient- adimensional unit), AIF (Angle of Internal Friction), BD (Bulk Density)

consistent across both samples, ensuring a comparable baseline for rheological evaluation. The Flow Function Coefficient (FFc), the primary parameter for characterizing powder flowability, categorized NCS as an 'easy-flowing' material ($4 < FFc < 10$), whereas the ESE modification shifted the classification to the 'free-flowing' regime ($FFc > 10$). Interestingly, the Angle of Internal Friction (AIF) showed negligible differences between the two powders, suggesting that the fundamental mechanical friction remains largely unaffected by the modification. While the Bulk Density (BD) of NCS aligned with previous findings, ESE exhibited a notably lower BD. This divergence is likely attributable to the lower intrinsic mass and higher air entrapment within the enzymatic powder matrix. In conclusion, the enzymatic modification of native corn starch effectively enhances powder flowability while simultaneously reducing cohesive behavior.

## 4. Conclusion

This study examined several strategies to produce different morphologies for corn, mung bean, and tapioca starches. The four techniques applied in this work included enzymatic hydrolysis, microprecipitation, spray-drying, and freeze-drying, which produced sheets, donuts, deflated spheres, and smooth starch particles, respectively. Enzymatic hydrolysis, in particular, involved the preferential erosion of the microparticle surface, which considerably enhanced flowability by reducing interparticle cohesion and unconfined yield strength, all while preserving the native chemical structure. On the other hand, microprecipitation can lead to the generation of donut-shaped and deflated spheres upon solubilization in an anti-solvent via polymer reorganization without chemical modification; similarly, there is also a need for polymer solubilization in spray-drying to form the deflated microspheres, though at the cost of a reduction in flowability. Freeze-drying generated sheet-like structures as water sublimated.

All procedures gave the corresponding products in good yields under friendly conditions, with no use of hazardous chemicals or organic solvents, and are industrially upscalable. Importantly, the starch chemical structure is preserved in every case. This aspect is crucial for cosmetic applications because these modified starches can be used without registration as a new ingredient in the International Nomenclature of Cosmetic Ingredients system (INCI). Retention of the native chemical structure provides an easy regulatory compliance situation, lowering the time and cost involved in testing safety, and accelerates formulation development. In other words, companies can benefit from the functional advantages presented by a novel particle morphology, like improved flowability, absorption of water, or texture, based on an already known and approved ingredient, which is much safer from the regulatory point of view. Our findings provide partial confirmation for the hypothesis that structured starch microparticles can replicate the tactile 'ball bearing effect' of synthetic microplastics. Specifically, only the enzymatically treated samples or ESE (producing smooth starch particles) demonstrated the necessary sphericity, particle size distribution, and low-friction profiles to rigorously match the benchmarking performance of synthetic microplastics. While the other three processing routes successfully preserved the native starch chemical structure (ensuring straightforward INCI compliance), they offered alternative functional properties (such as water absorption or specific texturizing profiles) rather than a direct replication of the microplastic tactile effect. Additionally, FT4 powder rheometry represents a highly sophisticated method for cosmetic characterization, this advanced analysis was performed exclusively on the ESE in comparison to native starch. Future studies will aim to extend this comprehensive rheological benchmarking to the other developed morphologies (such as donuts and deflated spheres) to fully map their behavior.

In this framework, this work underlines the versatility of natural starches as renewable raw materials and provides insights into the effectiveness of using morphology-dependent properties in applications like cosmetics. Consequently, the presented study opens new panoramas toward the exploitation of common carbohydrates innovatively and practically while reducing the gap between natural materials and their use in everyday industrial applications.

## CRediT authorship contribution statement

**Giulia Sinesi:** Writing – original draft, Visualization, Investigation, Formal analysis, Data curation. **Gaetano Distefano:** Writing – review & editing, Visualization, Validation, Supervision, Methodology, Investigation, Conceptualization. **Lucia Morelli:** Validation. **Lucia Salvioni:** Validation. **Patrizia Valsesia:** Writing – review & editing, Supervision, Resources, Funding acquisition, Conceptualization. **Davide Prosperi:** Writing – review & editing, Supervision, Resources, Funding acquisition, Conceptualization. **Marco Giustra:** Writing – review & editing, Writing – original draft, Supervision, Methodology, Investigation, Data curation, Conceptualization. **Miriam Colombo:** Writing – review & editing, Supervision, Resources, Funding acquisition, Conceptualization.

## Declaration of competing interest

The authors declare that they have no known competing financial interests or personal relationships that could have appeared to influence the work reported in this paper.

## Acknowledgement

This research was funded by 2021-ECO-0033/B—JOINTLAB UNIMIB-INTERCOS.

## Supplementary materials

Supplementary material associated with this article can be found, in the online version, at doi:10.1016/j.carpta.2026.101237.

## Data availability

Data will be made available on request.

## References

Abdelwahed, W., Degobert, G., Stainmesse, S., & Fessi, H. (2006). Freeze-drying of nanoparticles: Formulation, process and storage considerations. *Advanced Drug Delivery Reviews, 58*(15), 1688–1713. https://doi.org/10.1016/J.ADDR.2006.09.017

Abdullah, A. H. D., Chalimah, S., Primadona, I., & Hanantyo, M. H. G (2018). Physical and chemical properties of corn, cassava, and potato starchs. *IOP Conference Series: Earth and Environmental Science, 160*(1), Article 012003. https://doi.org/10.1088/1755-1315/160/1/012003

Ajayi, O. M., & Amin, S. (2021). Flow and performance effects of talc alternatives on powder cosmetic formulations. *International Journal of Cosmetic Science, 43*(5), 588–600. https://doi.org/10.1111/ICS.12733

Ascheri, J. L. R., Zamudio, L. H. B., Carvalho, C. W. P., Arevalo, A. M., & Fontoura, L. M. (2014). Extraction and Characterization of Starch Fractions of Five Phenotypes Pachyrhizus tuberosus (Lam.) Spreng. *Food and Nutrition Sciences, 05*(19), 1875–1885. https://doi.org/10.4236/fns.2014.519200

Baltrusch, K. L., Torres, M. D., Domínguez, H., & Flórez-Fernández, N. (2022). Spray-drying microencapsulation of tea extracts using green starch, alginate or carrageenan as carrier materials. *International Journal of Biological Macromolecules, 203*, 417–429. https://doi.org/10.1016/J.IJBIOMAC.2022.01.129

Bertolini, A. C. (2010). *Starches : characterization, properties, and applications*. 276.

Choi, Y., & Choi, K. Y. (2025). Indirubin-incorporated biodegradable PHB microbeads and its application for functional facial cleanser. *Dyes and Pigments, 235*, Article 112586. https://doi.org/10.1016/J.DYEPIG.2024.112586

Christen, M. O., & Vercesi, F. (2020). Polycaprolactone: How a Well-Known and Futuristic Polymer Has Become an Innovative Collagen-Stimulator in Esthetics. *Clinical, Cosmetic and Investigational Dermatology, 13*, 31–48. https://doi.org/10.2147/CCID.S229054

Ciurzyńska, A., & Lenart, A. (2011). Freeze-Drying - Application in Food Processing and Biotechnology - a Review. *Polish Journal of Food and Nutrition Sciences, 61*(3), 165–171. https://doi.org/10.2478/V10222-011-0017-5

Cubas, A. L. V., Bianchet, R. T., Reis, I. M. A. S.dos, & Gouveia, I. C. (2022). Plastics and Microplastic in the Cosmetic Industry: Aggregating Sustainable Actions Aimed at Alignment and Interaction with UN Sustainable Development Goals. *Polymers, 14* (21), 4576. https://doi.org/10.3390/POLYM14214576. *2022, Vol. 14, Page 4576*.

Emenike, P. C., Araoye, O. V., Academe, S. O., Unokiwedi, P., & Omole, D. O. (2022). The effects of microplastics in oceans and marine environment on public health – a mini-review. *IOP Conference Series: Earth and Environmental Science, 993*(1), Article 012019. https://doi.org/10.1088/1755-1315/993/1/012019

Enyoh, C. E., Devi, A., Kadono, H., Wang, Q., & Rabin, M. H. (2023). The Plastic Within: Microplastics Invading Human Organs and Bodily Fluids Systems. *Environments, 10* (11), 194. https://doi.org/10.3390/ENVIRONMENTS10110194

Enyoh, C. E., Shafea, L., Verla, A. W., Verla, E. N., Qingyue, W., Chowdhury, T., & Paredes, M. (2020). Microplastics Exposure Routes and Toxicity Studies to Ecosystems: An Overview. *Environmental Analysis, Health and Toxicology, 35*(1), Article e2020004. https://doi.org/10.5620/EAHT.E2020004

Falana, A., & Adenusi, A. A. (2026). Non-Newtonian Characterization of Gelatinized Corn Starch Dispersions with Magnetic Particle Enhancement Under Shear Stress. *International Journal of Research and Innovation in Applied Science (IJRIAS), 11*(2), 444–456. https://doi.org/10.51584/IJRIAS.2026.110200041. *Volume 11 Issue 2*.

Farrag, Y., Sabando, C., Rodríguez-Llamazares, S., Bouza, R., Rojas, C., & Barral, L. (2018). Preparation of donut-shaped starch microparticles by aqueous-alcoholic treatment. *Food Chemistry, 246*, 1–5. https://doi.org/10.1016/J.FOODCHEM.2017.10.147

Fu, Z. Q., Wang, L. J., Li, D., & Adhikari, B. (2012). Effects of partial gelatinization on structure and thermal properties of corn starch after spray drying. *Carbohydrate Polymers, 88*(4), 1319–1325. https://doi.org/10.1016/J.CARBPOL.2012.02.010

Gan, H., Okada, T., Kimura, S., Kasuya, K.ichi, & Iwata, T. (2023). Manufacture, physical properties, and degradation of biodegradable polyester microbeads. *Polymer Degradation and Stability, 208*, Article 110239. https://doi.org/10.1016/J.POLYMDEGRADSTAB.2022.110239

Giustra, M., Sinesi, G., Spena, F., De Santes, B., Morelli, L., Barbieri, L., Garbujo, S., Galli, P., Prosperi, D., & Colombo, M. (2024). Microplastics in Cosmetics: Open Questions and Sustainable Opportunities. *ChemSusChem, 17*(22), Article e202401065. https://doi.org/10.1002/CSSC.202401065

Gupta, S., Sharma, S., Kumar Nadda, A., Saad Bala Husain, M., & Gupta, A. (2022). Biopolymers from waste biomass and its applications in the cosmetic industry: A review. *Materials Today: Proceedings, 68*, 873–879. https://doi.org/10.1016/J.MATPR.2022.06.422

Hoover, R., Li, Y. X., Hynes, G., & Senanayake, N. (1997). Physicochemical characterization of mung bean starch. *Food Hydrocolloids, 11*(4), 401–408. https://doi.org/10.1016/S0268-005X(97)80037-9

Hsieh, C. F., Liu, W., Whaley, J. K., & Shi, Y. C. (2019). Structure, properties, and potential applications of waxy tapioca starches – A review. *Trends in Food Science & Technology, 83*, 225–234. https://doi.org/10.1016/J.TIFS.2018.11.022

Infante, V. H. P., Calixto, L. S., & Campos, P. M. B. G. M. (2024). Application of tapioca and corn starches as an alternative for synthetic polymers in cosmetic products. *Brazilian Journal of Pharmaceutical Sciences, 60*, Article e20124. https://doi.org/10.1590/S2175-97902024E20124

Ju, S., Shin, G., Lee, M., Koo, J. M., Jeon, H., Ok, Y. S., Hwang, D. S., Hwang, S. Y., Oh, D. X., & Park, J. (2021). Biodegradable chito-beads replacing non-biodegradable microplastics for cosmetics. *Green Chemistry, 23*(18), 6953–6965. https://doi.org/10.1039/D1GC01588E

Kaur, M., Sandhu, K. S., Singh, N., & Lim, S. T. (2011). Amylose content, molecular structure, physicochemical properties and in vitro digestibility of starches from different mung bean (Vigna radiata L.) cultivars. *Starch/Staerke, 63*(11), 709–716. https://doi.org/10.1002/STAR.201100053

Kittipongpatana, N., & Kittipongpatana, O. (2015). Cross-linked carboxymethyl mung bean starch as pharmaceutical gelling agent and emulsion stabilizer. *International Journal of Pharmacy and Pharmaceutical Sciences, 7*(1), 404–407.

Krystyjan, M., Dobosz-Kobędza, A., Sikora, M., & Baranowska, H. M. (2022). Influence of Xanthan Gum Addition on the Short- and Long-Term Retrogradation of Corn Starches of Various Amylose Content. *Polymers, 14*(3), 452. https://doi.org/10.3390/POLYM14030452. *2022, Vol. 14, Page 452*.

Kulshreshtha, Y., Schlangen, E., Jonkers, H. M., Vardon, P. J., & van Paassen, L. A. (2017). CoRncrete: A corn starch based building material. *Construction and Building Materials, 154*, 411–423. https://doi.org/10.1016/J.CONBUILDMAT.2017.07.184

Liew, K. Bin, Odeniyi, M. A., & Peh, K. K (2016). Application of freeze-drying technology in manufacturing orally disintegrating films. *Pharmaceutical Development and Technology, 21*(3), 346–353. https://doi.org/10.3109/10837450.2014.1003657

Lochhead, R. Y. (2007). The role of polymers in cosmetics: Recent trends. *ACS Symposium Series, 961*, 3–56. https://doi.org/10.1021/BK-2007-0961.CH001

Ma, A., Li, R., Bai, T., Sun, Y., Wang, L., Hou, D., & Zhou, S. (2025). Gluten-free whole mung bean noodles: Role of transglutaminase and hydrocolloids in their physicochemical, sensory, and in vitro starch digestion characteristics. *Journal of Future Foods*. https://doi.org/10.1016/J.JFUTFO.2025.09.035

Ma, H., Liu, M., Liang, Y., Zheng, X., Sun, L., Dang, W., Li, J., Li, L., & Liu, C. (2022). Research progress on properties of pre-gelatinized starch and its application in wheat flour products. *Grain & Oil Science and Technology, 5*(2), 87–97. https://doi.org/10.1016/J.GAOST.2022.01.001

Maktabi, B., Liberatore, M. W., & Baki, G. (2021). Meadowfoam seed oil as a natural dispersing agent for colorants in lipstick. *International Journal of Cosmetic Science, 43* (4), 484–493. https://doi.org/10.1111/ics.12724

Mazár, J., Albert, K., Kovács, Z., Koris, A., Nath, A., & Bánvölgyi, S. (2025). Advances in Spray-Drying and Freeze-Drying Technologies for the Microencapsulation of Instant Tea and Herbal Powders: The Role of Wall Materials. *Foods, 14*(3), 486. https://doi.org/10.3390/FOODS14030486. *2025, Vol. 14, Page 486*.

Min, C., He, M., Wang, R., He, C., Liu, M., Li, Y., Feng, L., & Cao, Y. (2026). Rheological, textural, and structural properties of heat-induced yam starch gels: Effects of high-amylose mung bean starch. *Food Chemistry: X, 36*, Article 104023. https://doi.org/10.1016/J.FOCHX.2026.104023

OECD. (1992). *Test No.301: Ready Biodegradability. OECD Guidelines for the Testing of Chemicals, Section 3*. Paris: OECD Publishing. https://doi.org/10.1787/9789264070349-en

Pardeshi, S. R., Deshmukh, N. S., Telange, D. R., Nangare, S. N., Sonar, Y. Y., Lakade, S. H., Harde, M. T., Pardeshi, C. V., Gholap, A., Deshmukh, P. K., & More, M. P. (2023). Process development and quality attributes for the freeze-drying process in pharmaceuticals, biopharmaceuticals and nanomedicine delivery: a state-of-the-art review. *Future Journal of Pharmaceutical Sciences, 9*(1), 99-. https://doi.org/10.1186/S43094-023-00551-8. *2023 9:1*.

Patel, R. P., Patel, M. P., & Suthar, A. M. (2009). Spray drying technology: an overview. *Indian Journal of Science and Technology, 2*(10), 44–47. https://doi.org/10.17485/IJST/2009/V2I10.3

Pérez, S., & Bertoft, E. (2010). The molecular structures of starch components and their contribution to the architecture of starch granules: A comprehensive review. *Starch - Stärke, 62*(8), 389–420. https://doi.org/10.1002/STAR.201000013

Petsitis, X. (2018). Microplastic in Cosmetics—Alternatives for the sensory Profile. *Euro. Cosmetics*, (10), 14–16.

Pozo, C., Rodríguez-Llamazares, S., Bouza, R., Barral, L., Castaño, J., Müller, N., & Restrepo, I. (2018). Study of the structural order of native starch granules using combined FTIR and XRD analysis. *Journal of Polymer Research, 25*(12), 266-. https://doi.org/10.1007/S10965-018-1651-Y. *2018 25:12*.

Punia Bangar, S., Ashogbon, A. O., Singh, A., Chaudhary, V., & Whiteside, W. S. (2022). Enzymatic modification of starch: A green approach for starch applications. *Carbohydrate Polymers, 287*, Article 119265. https://doi.org/10.1016/J.CARBPOL.2022.119265

Puri, A., Mohite, P., Ramole, A., Verma, S., Kamble, M., Ranch, K., & Singh, S. (2025). Starch Science Advancement: Isolation Techniques, Modification Strategies, and Multifaceted Applications. *Macromol, 5*(3), 40. https://doi.org/10.3390/MACROMOL5030040. *2025, Vol. 5, Page 40*.

Qin, Y., Liu, C., Jiang, S., Xiong, L., & Sun, Q. (2016). Characterization of starch nanoparticles prepared by nanoprecipitation: Influence of amylose content and starch type. *Industrial Crops and Products, 87*, 182–190. https://doi.org/10.1016/J.INDCROP.2016.04.038

Ravaghi, M., Sinico, C., Razavi, S. H., Mousavi, S. M., Pini, E., & Fadda, A. M. (2017). Proniosomal powders of natural canthaxanthin: Preparation and characterization. *Food Chemistry, 220*, 233–241. https://doi.org/10.1016/J.FOODCHEM.2016.09.162

Samanta, P., Dey, S., Kundu, D., Dutta, D., Jambulkar, R., Mishra, R., Ghosh, A. R., & Kumar, S. (2022). An insight on sampling, identification, quantification and characteristics of microplastics in solid wastes. *Trends in Environmental Analytical Chemistry, 36*, Article e00181. https://doi.org/10.1016/J.TEAC.2022.E00181

Schneider, L., & Gärtner, H. (2013). The advantage of using a starch based non-Newtonian fluid to prepare micro sections. *Dendrochronologia, 31*(3), 175–178. https://doi.org/10.1016/J.DENDRO.2013.04.002

Senanayake, S., Gunaratne, A., Ranaweera, K., & Bamunuarachchi, A. (2013). Effect of heat moisture treatment conditions on swelling power and water soluble index of different cultivars of sweet potato (Ipomea batatas (L). Lam) starch. *ISRN Agronomy, 2013*, 1–4. https://doi.org/10.1155/2013/502457

Shebalin, I. (2021). *Amorphous Mesoporous Magnesium Carbonate in cosmetics: Absorption and interaction with oils, soft-focus effect and transparency*.

Shoukat, R., Cappai, M., Pilia, L., & Pia, G. (2025). Rice starch chemistry, functional properties, and industrial applications: A review. *Polymers, 17*(1), 110. https://doi.org/10.3390/POLYM17010110. *2025, Vol. 17, Page 110*.

Siddiqui, N. A., Tauseef, S. M., Abbasi, S. A., & Khan, F. I. (Eds.). (2020). *Advances in air pollution profiling and control. springer transactions in civil and environmental engineering*. https://doi.org/10.1007/978-981-15-0954-4.

Sudesh, K., Bhubalan, K., Chuah, J. A., Kek, Y. K., Kamilah, H., Sridewi, N., & Lee, Y. F. (2011). Synthesis of polyhydroxyalkanoate from palm oil and some new applications. *Applied Microbiology and Biotechnology, 89*(5), 1373–1386. https://doi.org/10.1007/S00253-011-3098-5. *2011 89:5*.

Suhagia, T. A., Ayare, P., & Alle, M. (2025). Biodegradable beauty: Carbohydrate polymers in cosmetics. *Smart Nanomaterials Technology*, 455–483. https://doi.org/10.1007/978-981-96-2171-2_18

Suryani, M., Pariwisata, F., Perhotelan, D., Minerva, P., Rias, J. T., & Kecantikan, D. (2022). Feasibility of cornstarch masks for dry facial skin care. *Jurnal Tata Rias Dan Kecantikan, 4*(2), 102–108. https://doi.org/10.24036/JITRK.V4I2.105

Thakur, C., Kaushal, M., Vaidya, D., Verma, A. K., Gupta, A., & Sharma, R. (2024). Unlocking the potential of spray drying for agro-products: Exploring advanced techniques, carrier agents, applications, and limitations. *Food and Bioprocess Technology, 18*(2), 1181–1220. https://doi.org/10.1007/S11947-024-03544-4. *2024 18:2*.

The European Commission. (2023). Commission Regulation 2023/2055 of 25 September 2023 amending Annex XVII to Regulation (EC) n. 1907/2006 of the European Parliament and of the Council concerning the Registration, Evaluation, Authorisation and Restriction of Chemicals (REACH) as regards synthetic polymer microparticles. *Official Journal of the European Union, L238*, 67–88.

Tian, L., van Putten, R. J., & Gruter, G. J. M. (2022). Plastic pollution. The role of (bio) degradable plastics and other solutions. *Biodegradable Polymers in the Circular Plastics Economy*, 59–81. https://doi.org/10.1002/9783527827589.CH3

Ulyarti, U., Lisani, L., Surhaini, S., Lumbanraja, P., Satrio, B., Supriyadi, S., & Nazarudin, N. (2021). The application of gelatinisation techniques in modification of cassava and yam starches using precipitation method. *Journal of Food Science and Technology, 59*(3), 1230–1238. https://doi.org/10.1007/S13197-021-05134-0. *2021 59:3*.

United States Pharmacopeia. (2024). <1174>Powder Flow (Stage 4 Harmonization, Official May 1, 2024). *United States Pharmacopeia and National Formulary (USP-NF). United States Pharmacopeial Convention.*

Xu, Y., Chan, F. K. S., Johnson, M., Stanton, T., He, J., Jia, T., Wang, J., Wang, Z., Yao, Y., Yang, J., Liu, D., Xu, Y., & Yu, X. (2021). Microplastic pollution in Chinese urban rivers: The influence of urban factors. *Resources, Conservation and Recycling, 173*, Article 105686. https://doi.org/10.1016/j.resconrec.2021.105686

Zhong, Y., Xu, J., Liu, X., Ding, L., Svensson, B., Herburger, K., Guo, K., Pang, C., & Blennow, A. (2022). Recent advances in enzyme biotechnology on modifying gelatinized and granular starch. *Trends in Food Science & Technology, 123*, 343–354. https://doi.org/10.1016/J.TIFS.2022.03.019

Zhu, F. (2015). Composition, structure, physicochemical properties, and modifications of cassava starch. *Carbohydrate Polymers, 122*, 456–480. https://doi.org/10.1016/J.CARBPOL.2014.10.063